ChemEngineering

MDPI

Review

Bulk Perovskite Oxides: Synthesis, Structure–Property Relationships and Engineering Applications

Nurzada Totenova [1], Bakytgul Massalimova [2], Vladislav Sadykov [3,4], Gaukhar Abilmazhinova [5], Laura Nurlybay [5], Aisulu Kabylbekova [6], Dina Kitapbayeva [5], Zhazira Mukazhanova [5,*] and Akmaral Darmenbayeva [1,*]

1 Department of Chemistry and Chemical Technology, M.Kh. Dulaty Taraz University, Taraz 080000, Kazakhstan; ms.nurzada.93kz@mail.ru
2 Department of Chemistry and Chemical Technology, M. Kozybayev North Kazakhstan University, Petropavlovsk 150000, Kazakhstan; bkmasalimova@ku.edu.kz
3 Federal Research Center, Boreskov Institute of Catalysis SB RAS, Novosibirsk 630090, Russia; sadykov@catalysis.ru
4 Department of Natural Sciences, Novosibirsk State University, Novosibirsk 630090, Russia
5 Department of Chemistry, Higher School of IT and Natural Sciences, S. Amanzholov East Kazakhstan University, Ust-Kamenogorsk 070010, Kazakhstan; gaukhara70@mail.ru (G.A.); lrn19.98@mail.ru (L.N.); kitapbaeva75@mail.ru (D.K.)
6 Department of Chemistry, Biology and Physical Education, Miras University, Shymkent 160012, Kazakhstan; aika_kabil@mail.ru
* Correspondence: mukazhanovazhb@mail.ru (Z.M.); maral88.ad@gmail.com (A.D.); Tel.: +7-747-140-62-66 (Z.M.); +7-701-787-5389 (A.D.)

Abstract

Perovskite oxides have emerged as a versatile class of functional materials owing to their structural flexibility, tunable defect chemistry, mixed ionic–electronic conductivity, and excellent thermal stability. These characteristics make them attractive for engineering applications in heterogeneous catalysis, solid oxide fuel cells (SOFCs), oxygen separation membranes, and sustainable energy conversion. This review critically analyzes recent advances in the crystal structure, physicochemical properties, defect chemistry, synthesis strategies, and engineering applications of bulk perovskite oxides and related Ruddlesden–Popper phases. Conventional and advanced synthesis methods, including solid-state, sol–gel, Pechini, hydrothermal, solution combustion, and spray pyrolysis approaches, are compared with respect to compositional homogeneity, microstructure, oxygen vacancy formation, scalability, and functional performance. The review demonstrates that the performance of perovskite materials is governed by the interplay between crystal structure, defect chemistry, synthesis route, and oxygen mobility. Recent developments in methane reforming, catalytic oxidation, SOFC electrodes, oxygen separation membranes, and perovskite–fluorite nanocomposites highlight the broad engineering potential of these materials. Despite significant progress, challenges remain in achieving long-term structural stability, reproducible large-scale synthesis, and precise defect engineering. Future research should focus on sustainable manufacturing strategies, nanocomposite design, and data-driven materials optimization to accelerate the development of next-generation functional perovskite materials.

Keywords: bulk perovskite oxides; Ruddlesden–Popper oxides; functional oxide materials; synthesis methods; heterogeneous catalysis

Check for updates

Academic Editor: Dmitry Yu. Murzin

Received: 7 July 2026
Revised: 7 September 2026
Accepted: 17 September 2026
Published: 22 September 2026

Copyright: © 2026 by the authors. Licensee MDPI, Basel, Switzerland. This article is an open access article distributed under the terms and conditions of the Creative Commons Attribution (CC BY) license.

1. Introduction

The accelerating global demand for cleaner energy, the pressing need to mitigate greenhouse gas emissions, and the finite availability of fossil fuel reserves have led to an urgent push toward sustainable and efficient energy conversion technologies. In response to the environmental challenges articulated in frameworks such as the Paris Agreement, there is increasing focus on renewable energy strategies and advanced catalytic systems that can enable carbon-neutral or low-carbon pathways for power generation and chemical production [1].

Within this context, perovskite-type oxides with the general formula ABO_3 have attracted considerable attention as multifunctional materials for energy and environmental applications owing to their structural flexibility, redox properties, oxygen mobility, and thermal stability [2]. In addition to classical ABO_3 perovskites, layered Ruddlesden–Popper (R–P) oxides constitute an important family of perovskite-related materials. Their general formula is $A_{n+1}B_nO_{3n+1}$, which can also be expressed as $AO(ABO_3)_n$, where n perovskite layers are separated by rock-salt AO layers along the crystallographic c-axis [3]. As n approaches infinity, the structure gradually converges to the three-dimensional perovskite framework. The n = 1 member, represented by compounds such as $Ln_2NiO_{4+\delta}$, exhibits unique oxygen transport properties due to the presence of interstitial oxygen species and layered structural anisotropy [4]. Representative systems include rare-earth transition-metal perovskites ($LnMeO_3$, where Ln is a rare-earth element and Me is a transition metal) and layered nickelates of the Ruddlesden–Popper family. Their compositional flexibility enables tuning of catalytic, electrochemical, and oxygen-transport properties [2].

The interest in perovskite materials is rooted in their historical discovery—first identified in $CaTiO_3$ by Gustav Rose in 1839 and named after Count Lev Perovsky. The "perovskite" label has since expanded to include a wide family of ABX_3 compounds with versatile chemical compositions and coordination environments. Among these, oxide perovskites (ABO_3) are especially significant due to their thermal robustness, tunable band structure, and the ability to accommodate multiple oxidation states—key factors that determine catalytic and electrochemical performance [5]. These materials are distinguished by their structurally flexible crystal lattice, which accommodates extensive A- and B-site substitution, enabling fine-tuning of key physicochemical properties such as redox activity, ionic/electronic conductivity, and oxygen mobility [5–8]. These features underpin their applicability in diverse catalytic processes, including total and partial oxidation of methane and other hydrocarbons [9–12], CO oxidation [13], and reforming of hydrocarbons and biofuels into syngas [10,14–20]. Additionally, their high-temperature stability and ionic conductivity make them excellent candidates for solid oxide fuel cell (SOFC) electrodes and oxygen separation membranes [21–28].

A particularly valuable property of perovskites in steam and oxidative steam reforming of hydrocarbons and biofuel-derived compounds is their ability to form oxygen vacancies and facilitate in situ generation of finely dispersed active metal species, such as metallic nickel clusters, during thermal or reaction exposure. This structural versatility results in enhanced coke resistance and catalytic durability, two major challenges for conventional reforming catalysts [15,16]. Nickel-substituted perovskites, in particular, offer synergistic effects combining the redox capacity of the lattice with metallic Ni activity and oxygen replenishment from the host structure [17–20].

A range of synthetic techniques has been developed to tailor the composition, morphology, and defect structure of bulk and nanostructured perovskites. These include solid-state reactions, mechanical activation, sol–gel processes, solution combustion synthesis, and the Pechini method [10,28–34]. Each approach offers distinct advantages in controlling particle size, surface area, crystallinity, and dopant distribution. Notably, the Pechini method allows

molecular-level mixing and stoichiometric control, resulting in nanostructured perovskites with superior catalytic performance.

Despite substantial progress, several challenges remain, particularly maintaining structural and chemical stability under operational conditions and optimizing oxygen transport and surface reactivity [2,35]. Further progress also requires scalable synthesis strategies capable of providing reproducible control over composition, defect chemistry, and microstructure. Addressing these issues requires a fundamental understanding of the interplay between composition, structure, defect chemistry, surface evolution, and function across different application scenarios.

This review provides a critical analysis of recent advances in perovskite-type oxides by linking synthesis strategies with crystal structure, defect chemistry, surface state, and functional performance. Here, the term "bulk perovskite oxides" refers to materials whose functional behavior originates from a three-dimensional perovskite or perovskite-related oxide lattice, irrespective of whether the resulting particles are micro- or nanoscale; it is used to distinguish these materials from thin-film and molecular perovskite systems rather than to imply that surface phenomena are negligible. Particular attention is given to the interdependence of these factors and to the limitations of interpreting individual descriptors, such as particle size, oxygen-vacancy concentration, or bulk composition, as independent predictors of performance. Representative examples from catalysis, SOFCs, oxygen separation, and high-entropy perovskites are compared to identify recurring structure–property–activity relationships, key trade-offs, and remaining mechanistic limitations. This integrated perspective is used to formulate practical design considerations and priorities for future perovskite materials development.

2. Structure of Perovskites Results

2.1. Perovskites

The crystal structure of perovskite-type oxides has attracted considerable interest due to its exceptional ability to accommodate a wide variety of chemical compositions and structural distortions. The structure is based on a three-dimensional framework composed of BO_6 octahedra connected via shared oxygen atoms at the corners, forming a robust yet highly flexible network. This connectivity and geometric arrangement are illustrated in Figure 1. In this configuration, the larger A-site cation occupies the cuboctahedral void formed between the octahedra. Although the ideal symmetry is cubic (space group Pm $\bar{3}$ m), many perovskites crystallize in distorted forms such as orthorhombic, rhombohedral, or tetragonal phases depending on the ionic radii and oxidation states of the constituent elements [6].

The composition of perovskite can be modified by the partial substitution of cations in both A and B positions. ABO_3 oxides are initially regarded as purely ionic crystals. In the case of an ideal structure, the following relations between the radii of A, B, and O^{2-} ions are present:

$$r_A + r_O = \sqrt{2}(r_B + r_O) \quad (1)$$

where r_A, r_B, and r_O are the ionic radii of the A-site cation, B-site cation, and oxygen anion, respectively.

The ability of the perovskite lattice to tolerate a wide range of ionic substitutions is quantified by the Goldschmidt tolerance factor (t), which reflects the geometric fit of the A- and B-site cations with respect to the oxygen framework:

$$t = \frac{r_A + r_O}{\sqrt{2}(r_B + r_O)} \quad (2)$$

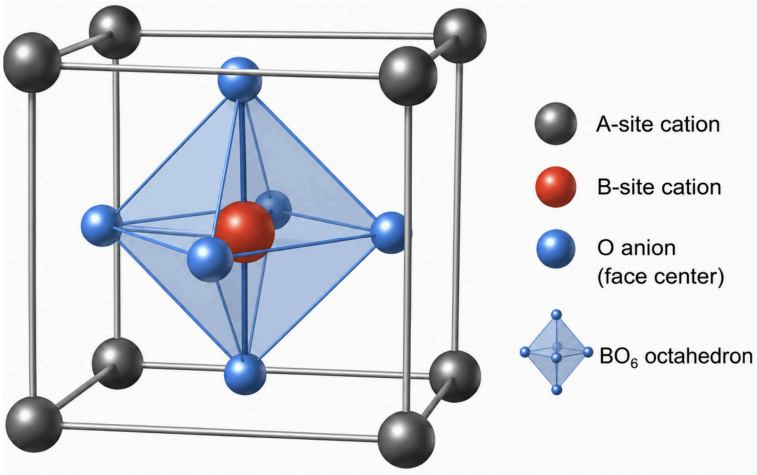

Figure 1. Schematic representation of the ideal cubic perovskite structure (ABO_3), showing A-site cations at cube corners (black), B-site cation at the center (red), and O anions at cube face centers (blue). BO_6 octahedra form a corner-sharing three-dimensional framework. The grey lines indicate the boundaries of the cubic unit cell.

A value of t close to 1 indicates a perfect cubic arrangement, while values below or above this threshold lead to tilting and distortion of the BO_6 octahedra. These distortions have significant implications for the physicochemical properties of perovskites, especially ionic and electronic conductivity [7]. These distortions influence the B–O–B bond angles and orbital overlap, which in turn affect the electronic conductivity and the mobility of oxygen species within the lattice.

The geometry of the lattice determines the permissible distortions within the limits of the tolerance factor change from 0.8 to 1. Due to the difference in the properties of cations B and B′/A and A′, the number of oxygen vacancies in the substituted perovskite can increase several times. As a consequence, such systems have significantly higher oxygen mobility compared to unsubstituted perovskites [8].

Concretely, lower tolerance factors ($t < 0.95$) are often associated with stronger octahedral tilting, which can reduce electronic conductivity due to decreased orbital overlap. However, moderate distortion may enhance surface reactivity by creating undercoordinated sites and increasing oxygen vacancy formation, thereby improving catalytic activity in oxidation reactions such as CO or CH_4 oxidation. Conversely, very low t values may destabilize the structure or impair oxygen mobility, leading to diminished performance. Thus, maintaining an optimal range of t (typically 0.9–1.0) is essential for balancing structural stability with a high catalytic efficiency.

A vivid illustration of the influence of the degree of structural distortion on the electrical conductivity is the dependence of the metal–semiconductor transition temperature in $RNiO_3$ perovskites on the type of rare earth element (R) cation. In these phases, with a decrease in the radius of the RZE cation and, accordingly, with an increase in the degree of distortion of the perovskite structure, an increase in the transition temperature to a state with metallic conductivity from 135 (Pr) to 403K (Sm) is observed. As follows from this, oxides with large cations of rare earth metals (La, Ce and Pr) should have the highest electrical conductivity among RBO_3 perovskites. The characteristic oxidation states of the last two elements are +3 and +4. Compounds containing Pr^{3+} are sufficiently stable, while those containing Ce^{3+} are unstable in an oxidizing atmosphere. The model of the zone structure of the ABO_3 perovskite is shown in Figure 2.

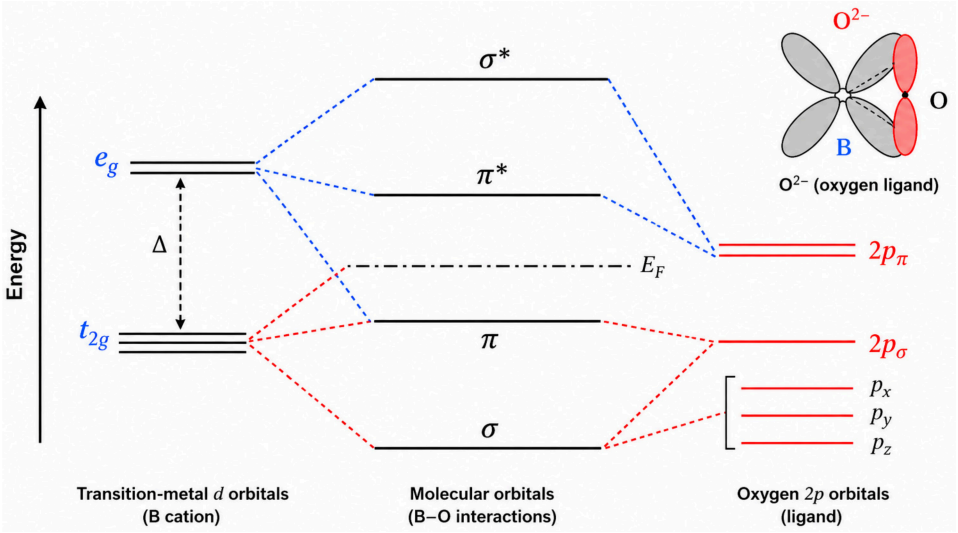

Figure 2. Schematic molecular-orbital representation of the interaction between transition-metal B-site d orbitals and O^{2-} 2p ligand orbitals in an ABO_3 perovskite. Blue and red dashed lines indicate contributions from B-site d and oxygen 2p orbitals, respectively; Δ denotes crystal-field splitting, and EF represents the Fermi level.

The upper right corner shows the overlap of the t_{2g} orbitals of the B cation and the $2p_\pi$ orbitals of oxygen during formation of the π* zone. The position of the Fermi level (E_F) is given for the case when the B-cation has two valence d-electrons (the π*-zone is filled by 1/3).

Among rare-earth-containing perovskites, Pr-based compositions often exhibit enhanced electronic conductivity due to favorable electronic interactions between Pr and O orbitals. In contrast, the stability of Ce-containing compounds may be limited under oxidizing conditions. Consequently, manganese-, cobalt-, and nickel-containing perovskites remain among the most attractive compositions for high-temperature catalytic and electrochemical applications [23,24].

2.2. Ruddlesden-Popper Structures

Complex oxides with R-P structures containing both perovskite-type $LnMeO_3$ layers and NaCl-type LnO layers (Figure 3) are now also considered as promising materials for the green energy field due to their high total conductivity and oxygen mobility provided by a cooperative mechanism of oxygen migration with participation of both interstitial oxygen species and apical oxygen in Me-O octahedra [36–40]. Their transport properties can be tuned by substitution in both cation sublattices depending upon the size and charge of doping cations and their content, affecting the concentration of oxygen interstitials as well as migration barriers due to the size of the dopant, Me-O length, and distortion of oxygen octahedra [3,39,41]. The most important advantage is that, in contrast to traditional $LnMO_3$ perovskites, these oxides possess a high total conductivity and oxygen mobility even without doping by alkaline earth cations, which cause a lot of problems during operation in realistic conditions due to formation of surface carbonates in catalysts and SOFC electrodes, interaction with doped zirconia electrolytes forming isolating layers of Ln, Ca (Sr) zirconates, etc. [10,21,28].

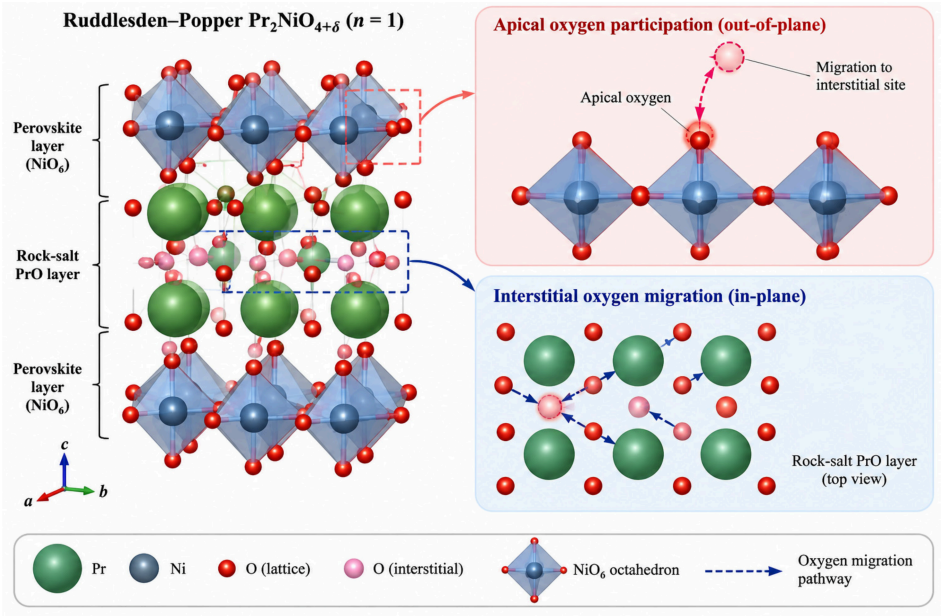

Figure 3. Schematic representation of the Ruddlesden–Popper $Pr_2NiO_{4+\delta}$ structure and the cooperative oxygen migration mechanism involving interstitial oxygen species and apical oxygen in NiO_6 octahedra.

3. Physicochemical Properties

The unique physicochemical properties of perovskite oxides, including mixed ionic–electronic conductivity, oxygen nonstoichiometry, redox flexibility, and structural tunability, underpin their broad application in catalysis, electrochemical energy conversion, and membrane technologies.

This flexibility provides perovskites with the following non-trivial properties:

1. Due to the ability of the transition metal to be in several degrees of oxidation, depending on external conditions, perovskites are able to accumulate oxygen nonstoichiometry. It is more correct to write the perovskite formula in the form of $ABO_{3-\delta}$, where the delta indicates a deviation from the ideal composition in real samples and theoretically can vary in the range $0 \leq \delta \leq 1$ [42]. As a result, such defective structures have oxygen mobility and are able to generate active oxygen on the surface. The high mobility of lattice oxygen in defect-rich perovskites facilitates oxygen transport toward the surface and can suppress carbon accumulation under reforming conditions [43].
2. Under reducing atmospheres, perovskites can undergo partial cation segregation, leading to the formation of defective structures decorated with highly dispersed metal nanoparticles firmly anchored on the oxide surface. This phenomenon enhances the catalytic functionality of the material by providing active metal–oxide interfaces.
3. The composition of perovskites can be finely tuned through partial substitution of cations at both A- and B-sites. Such substitution modifies the local structural environment, electronic structure, and defect chemistry and therefore provides an effective strategy for controlling catalytic activity, electronic conductivity, and oxygen transport.

A key structural characteristic of perovskites is their ability to form nonstoichiometric compositions, commonly represented as $ABO_{3-\delta}$, where δ denotes the concentration of oxygen vacancies. These defects play a crucial role in determining the catalytic and transport properties of the material by enhancing oxygen ion conductivity and facilitating lattice oxygen mobility. Oxygen vacancies can be controlled through aliovalent substitution at either the A- or B-site. For example, replacing La^{3+} with Sr^{2+} in $LaMnO_3$ promotes the

formation of Mn^{4+} species and oxygen vacancies to maintain charge neutrality. As a result, oxygen-deficient perovskites exhibit improved oxidation activity, enhanced resistance to carbon deposition, and superior performance in applications such as oxygen separation membranes, solid oxide fuel cells, and high-temperature oxidation catalysis [10,25]. In addition to defect chemistry, the electronic properties of perovskites are governed by the presence of mixed-valence B-site cations. In systems such as $LaCoO_3$ and $LaFeO_3$, the coexistence of multiple oxidation states facilitates charge transport through small-polaron hopping mechanisms, while in doped compounds such as $La_{1-x}Sr_xMnO_3$, Mn^{3+}/Mn^{4+} redox couples further enhance electronic conductivity and redox activity [10]. Overall, the available evidence indicates that no single structural parameter can fully explain the functional performance of perovskite oxides. Although tolerance factor, oxygen vacancy concentration, and mixed-valence states are often considered independently, their combined influence determines oxygen transport, redox behavior, and catalytic activity. Consequently, rational design of advanced perovskites requires simultaneous optimization of crystal structure, defect chemistry, and electronic properties rather than modification of a single structural descriptor.

An important distinction must therefore be made between bulk descriptors and the actual surface state under operating conditions. Bulk composition, crystal symmetry, tolerance factor, and oxygen nonstoichiometry define the thermodynamic and defect-chemical framework of a perovskite, but they do not necessarily identify the catalytic active sites. Under reducing, oxidizing, or reactant-rich environments, the surface may undergo cation segregation, reconstruction, exsolution of B-site species, and changes in oxygen-vacancy concentration and metal oxidation states [35,44]. Adsorbates may further modify surface coordination and redox states. Consequently, the composition and structure of the working surface can differ substantially from those of the as-synthesized bulk phase [45,46]. Bulk descriptors should therefore be interpreted as factors governing the accessibility and evolution of active surface states rather than as direct, universal predictors of catalytic activity.

The hybridization between the B-site transition metal d orbitals and the oxygen 2p orbitals leads to the formation of wide conduction and valence bands. This electronic structure can be fine-tuned by substitution, leading to either *p*-type or n-type semiconducting behavior. In $LaNiO_3$, for example, strong hybridization between Ni 3d and O 2p orbitals results in metallic conductivity and high redox flexibility, which is ideal for catalytic oxidation reactions [17–19].

Another crucial feature is the relationship between the structural distortion and the electronic phase behavior. The $RNiO_3$ (R = rare earth) series provides a classic example, where decreasing the ionic radius of the R-site cation increases the structural distortion, leading to a shift in the metal-insulator transition temperature. In $PrNiO_3$, the transition occurs at 135 K, whereas in $SmNiO_3$ it occurs above 400 K [23]. This structural tuning allows researchers to manipulate the material's electronic response for thermoelectric, magnetic, and catalytic applications.

Advanced characterization techniques such as X-Ray and neutron diffraction, synchrotron X-ray absorption spectroscopy, high-resolution transmission electron microscopy with surface elemental analysis (EDX), X-ray photoelectron spectroscopy (XPS), and Fourier-transformed Infrared Spectroscopy (FTIRS) of adsorbed test molecules (CO and NO) enabled detailed investigations of the structure, defect chemistry of perovskites and their surface properties [3,5,6,10,33,37,39–41,47].

At the nanoscale, perovskites prepared by modern advanced methods (plasmochemical decomposition, solution combustion, Pechini method, etc.) often exhibit increased surface area and defect density, which further enhances their catalytic efficiency. Nanosized

perovskites tend to stabilize high-energy surface terminations and expose active facets as well as outlets of extended defects (stacking faults, dislocations, twin and grain boundaries), increasing the number of available reaction sites able to stabilize reactive terminal oxygen species. These properties are particularly important in reactions involving complex multi-step mechanisms such as CO and methane oxidation, ammonia oxidation, steam reforming of fuels, and water-gas shift reactions [14,48].

In a similar way, perovskite-like oxides with Ruddlesden-Popper structure prepared by such methods as solution combustion and Pechini route demonstrate a high dispersion and spatial homogeneity of element distribution in nanodomains, along with a substantial amount of interstitial oxygen species controlled by doping [37,39,40].

Thus, the structural richness of perovskite oxides as well as oxides with R-P structure lies in their ability to combine geometric distortion, oxygen nonstoichiometry, and electronic complexity. These features can be synergistically engineered to enhance catalytic activity, thermal stability, and conductivity. As a result, perovskite-like complex oxides remain at the forefront of materials research for clean energy technologies, including heterogeneous catalysis, fuel cells, and membrane reactors.

Structural stability and defect chemistry jointly determine the long-term performance of perovskite oxides. While oxygen vacancies and interstitial species enhance ionic transport and catalytic activity, excessive defect concentrations may destabilize the lattice and promote phase transformations. Therefore, the optimal performance of perovskite-based materials is achieved through a balance between structural robustness and defect-assisted oxygen mobility [49–52].

Particle size is a critical parameter influencing the catalytic performance of perovskite-type oxides, particularly in reactions susceptible to carbon deposition such as methane reforming or CO hydrogenation. Smaller particles typically offer higher surface area-to-volume ratios, which increase the density of reactive surface sites and oxygen vacancy exposure. This enhances oxygen mobility, facilitating continuous lattice oxygen replenishment and, thereby, improving resistance to carbon buildup [53]. Particle size should, however, be distinguished from crystallite size: particle size describes the physical dimensions of individual particles or aggregates, typically determined by microscopic or particle-sizing techniques, whereas crystallite size refers to coherently diffracting crystalline domains commonly estimated from X-ray diffraction. Moreover, nanocrystalline perovskites exhibit shorter diffusion paths for oxygen ions and can accommodate dynamic redox cycles more efficiently than their bulk counterparts. Studies have shown that perovskite catalysts with average particle sizes below 50 nm demonstrate significantly improved coke resistance, attributed to their higher capacity for surface oxygen exchange and rapid regeneration of active sites [54]. For example, Isupova et al. demonstrated that the catalytic performance of $La_{1-x}Ca_xMnO_3$ perovskites is strongly influenced by their real structure and defect distribution, which are closely related to particle size and preparation conditions [55]. Similarly, Arapova et al. reported that highly dispersed perovskite–fluorite nanocomposites exhibited enhanced activity and stability in ethanol steam reforming due to improved oxygen mobility and developed interphase boundaries [56]. These observations confirm that reducing particle size and increasing structural homogeneity can significantly improve catalytic efficiency and resistance to deactivation. Nevertheless, particle size alone cannot be considered a universal descriptor of catalytic activity. Numerous studies have shown that catalysts with similar crystallite sizes may exhibit markedly different performance due to variations in defect concentration, oxygen mobility, surface composition, and metal–support interactions. Therefore, particle size and crystallite size should be interpreted as distinct descriptors and considered together with structural and electronic characteristics when designing advanced perovskite catalysts.

However, excessively small particles may suffer from sintering under high-temperature conditions, which diminishes their structural stability and catalytic performance over prolonged operation [45,57]. Therefore, a balance between nanoscale dispersion and thermal robustness is essential for designing perovskite materials with sustained catalytic activity and resistance to deactivation.

This intricate balance between defect chemistry and structural stability forms the foundation for the structure–property–activity relationships in perovskite and Ruddlesden–Popper-type oxides. Crystal structure, particularly the symmetry and distortion of the BO_6 octahedra, governs the electronic bandwidth, redox flexibility, and ionic transport. For instance, deviation from the ideal cubic symmetry through octahedral tilting or A-site mismatch can reduce electronic conductivity by altering B–O–B bond angles, while simultaneously promoting localized redox centers that enhance catalytic activity [58]. Such distortions influence the overlap between transition-metal d-orbitals and oxygen p-orbitals, impacting the position of the oxygen p-band center—a key descriptor correlated with oxygen evolution and reduction reaction (OER/ORR) activities [59].

Furthermore, oxygen vacancy formation energy, which is intimately linked to the lattice structure and cationic environment, determines the material's capacity to support fast oxygen ion transport and Mars–van Krevelen-type redox mechanisms. Studies have demonstrated that materials with intermediate oxygen vacancy formation energies exhibit optimal catalytic activity, reflecting a volcano-type relationship [60]. One widely used electronic descriptor, the egg orbital filling of the B-site cation, has been shown to correlate strongly with OER activity, where values close to unity (e.g., in $LaNiO_3$ or $Ba_{0.5}Sr_{0.5}Co_{0.8}Fe_{0.2}O_{3-\delta}$) promote the best performance [61].

Overall, the functional properties of perovskite oxides emerge from the coupled effects of crystal structure, electronic configuration, defect chemistry, and microstructure. Since these characteristics are strongly influenced by the preparation route, the following section examines the principal synthesis strategies used to control perovskite properties.

4. Synthesis Methods

Synthesis of perovskite-like materials with desired properties is one of the key tasks in the field of inorganic and materials chemistry. The choice of synthesis method directly affects the phase composition, crystallinity, morphology, defect structure and surface characteristics of the resulting compound, which in turn determines its catalytic, electrochemical and physical activity.

Perovskite oxides can be obtained in various ways with the general formula ABO_3—from traditional ceramic routes to modern low-temperature and chemical approaches. The methods include both high-temperature solid-phase synthesis [28] and soft chemical techniques such as sol–gel, autoclave (hydrothermal) procedures, combustion and spray pyrolysis [29–34].

Modern synthesis strategies focus on controlling crystallite size, defect concentration, compositional homogeneity, and surface reactivity, which are critical for catalytic, electrochemical, and membrane applications.

1. Solid sintering method. The classical route for preparing perovskite oxides involves high-temperature reactions between solid precursors such as oxides, carbonates, or nitrates. Due to diffusion limitations, repeated grinding and prolonged calcination are typically required. Although this method is simple, reproducible, and readily scalable, it generally produces materials with low surface areas (~1 m^2/g), relatively large particle sizes, and limited control over morphology and stoichiometry [28–30].
2. Sol–gel method. The sol–gel route is one of the most widely used approaches for the preparation of complex oxide materials. It involves hydrolysis and polycondensation

reactions of molecular precursors, resulting in highly homogeneous multicomponent systems. Compared with conventional solid-state synthesis, this approach enables lower processing temperatures, improved compositional homogeneity, and enhanced control over particle size and morphology. Consequently, nanostructured perovskites with specific surface areas of up to 20 m^2/g can be obtained. However, successful implementation requires careful control of synthesis parameters and relatively complex processing procedures [32].

Despite its widespread application, the sol–gel route cannot be regarded as universally superior to conventional solid-state synthesis. Although improved homogeneity and higher surface areas often translate into enhanced catalytic performance, increased process complexity and limited scalability may restrict industrial implementation. Therefore, the selection of a synthesis strategy should be based on the intended application and the required balance between material performance and manufacturing feasibility.

3. The Pechini method. The Pechini method is a widely used soft-chemistry route for the synthesis of multicomponent oxide materials with controlled stoichiometry and high compositional homogeneity [10,33]. The approach is based on the complexation of metal cations by citric acid, followed by polymerization with ethylene glycol to form a homogeneous organic network in which the metal ions are uniformly distributed (Figures 4 and 5). Subsequent thermal treatment removes the organic matrix and promotes the formation of the desired oxide phase.

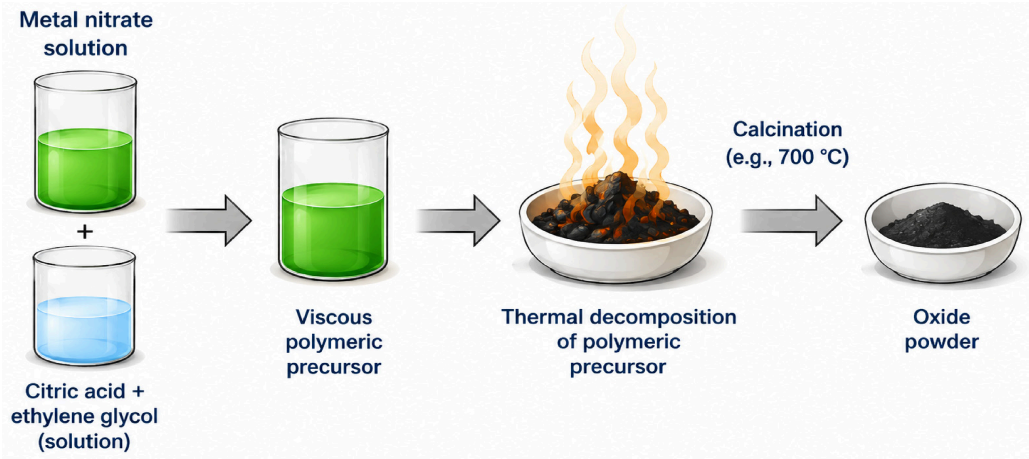

Figure 4. Scheme of synthesis of complex oxides by the modified Pechini method.

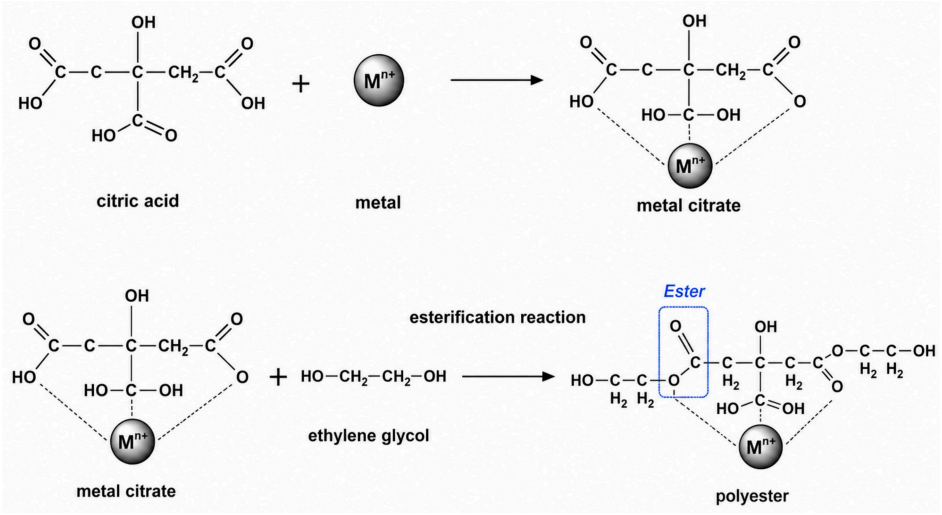

Figure 5. The diagram of the formation of a cation ester using citric acid and ethylene glycol.

In the presence of a polybasic alcohol, for example ethylene glycol, these complexes will react with alcohol molecules to form organic esters and water as reaction products.

Ethylenediamine is added for additional polymerization of the system by crosslinking amino groups with the remaining acid groups (Figure 5).

A major advantage of the Pechini route is the molecular-level mixing of precursors, which minimizes cation segregation and facilitates the formation of crystalline perovskite phases at relatively low temperatures. As a result, nanostructured materials with high surface areas, often reaching 60 m^2/g, can be obtained [10,33]. These characteristics are particularly beneficial for catalytic and electrochemical applications, where high dispersion and defect concentrations are desirable.

However, successful implementation of the Pechini method requires careful control of precursor composition and processing conditions. In addition, the use of organic reagents may result in residual carbon species after calcination, while the complexity of the process can limit large-scale industrial application.

The comparative table (Table 1) summarizes the main characteristics of three common methods for the synthesis of ABO_3 perovskite oxides: the solid-phase method, the sol–gel method, and the Pechini method. The table presents the parameters of synthesis temperature, degree of homogeneity, particle size, complexity of the technological process, possibilities for morphology control, the need to use organic reagents, and the scalability of the processes.

Table 1. General characteristics and processing considerations of representative synthesis routes for ABO_3 perovskite oxides.

Characteristic	Solid-State	Sol–Gel	Pechini
Typical synthesis temperature	Generally higher (often ~900–1400 °C)	Generally lower than solid-state (~500–900 °C)	Generally lower than solid-state (~500–900 °C)
Compositional homogeneity	Limited by solid-state mixing and diffusion	Improved by solution-level mixing	High degree of mixing through metal–citrate complexation
Powder characteristics	Generally coarser particles/agglomerates	Fine/nanoscale powders can be obtained	Fine and compositionally uniform powders can be obtained
Process requirements	Mixing/grinding and high-temperature treatment	Solution preparation, gelation, drying and calcination	Complexation, polymerization, organic removal and calcination
Morphology/microstructure control	Mainly controlled by milling and thermal treatment	Tunable through solution chemistry and thermal treatment	Tunable through precursor chemistry and thermal treatment
Scale-up considerations	Relatively straightforward but energy-intensive	More complex due to wet processing and drying	More complex due to organic precursor processing and decomposition
Examples	$LaMnO_3$, $SrTiO_3$	$LaFeO_3$, $BaTiO_3$	$La_{0.6}Sr_{0.4}CoO_{3-\delta}$, LSCF
Representative references	[31]	[32]	[27]

Although the Pechini and sol–gel methods generally provide higher homogeneity and smaller crystallite sizes than conventional solid-state synthesis, the literature data do not indicate a universally superior route. Pechini-derived perovskites frequently exhibit higher surface areas and enhanced catalytic activity due to molecular-level mixing of precursors and improved stoichiometric control. However, residual carbon species, the use of

organic reagents, and limited scalability remain important drawbacks. Similarly, the sol–gel method enables the preparation of nanostructured perovskites with high compositional homogeneity and moderate surface areas, although the process requires careful control of synthesis parameters and involves relatively complex processing steps. In contrast, solid-state synthesis offers excellent reproducibility, simplicity, and industrial scalability, but typically produces materials with larger particle sizes, lower surface areas, and reduced oxygen mobility. Therefore, the optimal synthesis route depends not on a single performance criterion but on the intended application, balancing catalytic activity, structural homogeneity, scalability, and production cost.

In addition to the three most widely used approaches summarized in Table 1, alternative preparation routes such as co-precipitation, hydrothermal synthesis, solution combustion, spray pyrolysis, microwave-assisted processing, and molten-salt synthesis have also been successfully applied for the preparation of perovskite oxides. These techniques offer specific advantages, including improved morphology control, shorter synthesis times, lower processing temperatures, and enhanced compositional homogeneity. At the same time, they may present limitations related to equipment requirements, process complexity, scalability, or reproducibility. Consequently, no single preparation strategy can be regarded as universally optimal, and the choice of synthesis route should be guided by the target application and the desired physicochemical characteristics of the material.

4. Preparation of nanocomposites with spinel and fluorites. High-temperature sintering of perovskite oxides often leads to grain growth and a substantial reduction in surface area, which is detrimental for catalytic applications. While this limitation can be addressed by depositing perovskites onto thermally stable supports, such as doped $MgAl_2O_4$ spinels or ceria-based oxides [10], electrochemical applications require a different strategy. For SOFC electrodes and oxygen separation membranes, improved performance is commonly achieved through the formation of nanocomposites combining perovskite phases with oxide-ion conductors such as doped ceria or ceria–zirconia [24,32].

The incorporation of fluorite or spinel phases promotes the formation of highly dispersed nanostructures with developed interphase boundaries. These interfaces facilitate oxygen transport, enhance oxygen mobility, and improve both catalytic activity and resistance to carbon deposition. Perovskite–fluorite nanocomposites have demonstrated particularly promising performance in ethanol steam reforming, SOFC cathodes, and oxygen separation membranes due to the synergistic interaction between the constituent phases [25,33].

Recent advances in microwave-assisted and radiation-thermal processing have further improved the fabrication of such nanocomposites by enabling lower sintering temperatures, finer microstructures, and more extensive interfacial regions, thereby enhancing oxygen transport and electrochemical performance [3,55].

Thus, the choice of synthesis route depends on the intended application. Conventional solid-state synthesis remains attractive for large-scale production, whereas sol–gel, Pechini, and nanocomposite-based approaches are generally preferred for catalysts, SOFC electrodes, and oxygen separation membranes due to their superior control of microstructure, oxygen mobility, and functional performance.

In addition to conventional solid-state, sol–gel, and hydrothermal methods, advanced synthesis routes such as microwave-assisted and molten-salt synthesis have recently attracted considerable attention. Microwave-assisted processing provides rapid and uniform heating, reducing reaction times and energy consumption while promoting the formation of nanostructured perovskites with enhanced redox properties [62,63]. Similarly, molten-salt synthesis enables the preparation of phase-pure perovskites at lower temperatures with controlled particle growth and morphology. These methods offer scalable and energy-

efficient alternatives for the production of perovskite materials intended for catalytic and electrochemical applications [64,65].

The synthesis strategy largely determines the crystal structure, particle size, defect concentration, and oxygen mobility of perovskites. These structural characteristics directly govern their catalytic behavior, making it important to consider how different compositions perform in representative catalytic reactions.

5. Catalytic Applications

Perovskite oxides ABO_3 attract considerable attention in heterogeneous catalysis due to their unique combination of properties: variable oxidation state of transition metals, ability to exhibit oxygen non-stoichiometry, high thermal stability, and adjustable surface activity. These materials exhibit both acid–base and redox properties, making them versatile catalysts for a wide range of reactions, including oxidative reforming, catalytic combustion, and electrochemical processes [66–68].

Of particular interest are the possibilities of structural and electronic modification of perovskites by doping, creation of oxygen vacancies and controlled formation of nano-sized metal phases in their volume. Such changes allow targeted influence on active centers and oxygen behavior in the lattice, increasing catalytic efficiency and resistance to deactivation [68,69].

Owing to these structural and electronic characteristics, perovskites have become versatile catalysts for a broad range of heterogeneous reactions. First of all, the efficiency of using perovskite-based catalysts in oxidative reactions for partial oxidation and dry reforming of methane, for which coke formation is the main cause of deactivation, was demonstrated. Perovskite-based catalysts require preliminary activation, and the metal-oxide active nanocomposite is formed in a reducing medium with partial or complete release of cations from the lattice. The stability to coke formation for catalysts obtained from perovskite precursors is explained by the high dispersion of metal particles, leading to a decrease or inhibition of coke formation in accordance with the theory of ensembles, as well as oxygen mobility, contributing to the oxidation of coke precursors. The main advantage of structured catalysts in comparison with granular catalysts is the high efficiency of mass transfer with a low hydraulic resistance, which allows the process to be carried out at short contact times. In this regard, it is possible to reduce the dimensions of the reactor and reduce the required amount of catalyst without reducing productivity. Similar technologies are being actively developed for biofuel transformation reactions into synthesis gas and hydrogen [17,70–75].

In addition to the high activity in desired reactions, the catalysts for such processes must be compatible with the materials of the structured carrier (or the anode of the fuel cell) and firmly fixed on their surface. Various structured carriers can be used as the basis of monolithic catalysts for biofuel transformation: ceramic [55,76].

In recent years, technologies for the manufacture of spatially structured carbon-based foam carriers have appeared, in which the surface is protected by applying a layer of metal and/or oxide that is stable under working conditions. Such carriers have a high thermal conductivity, electrical conductivity, unique strength characteristics, low specific gravity and compatibility with various types of materials (metals, oxides, etc.) [76]. As metals compatible with carbon, using nickel is the most promising, and as a protective oxide—corundum.

Manufacturing and testing in pilot reactors of structured catalysts based on active components that have previously shown good results in dilute mixtures in the form of fractions is the next step towards the industrial implementation of the technology and allows determining the compatibility and evaluating the efficiency and stability of the catalytic system when operating under real conditions.

The range of applications of these catalysts is extremely wide and diverse: steam reforming of oxygenates [70], neutralization of automobile engine emissions, partial oxidation of hydrocarbons and oxygen-containing compounds, photocatalysis, reduction of sulfur dioxide, oxidative dimerization of methane, decomposition of hydrogen peroxide, oxidation of CO and hydrocarbons.

Methane oxidation has been extensively investigated on La-containing perovskites with the general formula $LaBO_3$ (B = Cr, Mn, Fe, Co, Ni) and partially substituted compositions $La_{1-x}Sr_xBO_3$. The catalytic activity was found to follow the sequence Ni > Fe, Mn, Co > Cr, while substitution of La by Sr generally enhanced catalytic performance, with the most pronounced effect observed for $LaMnO_3$ [77]. Depending on the perovskite composition, the activation energy varied from 59 to 134 kJ mol^{-1}.

Experimental studies demonstrated that methane oxidation proceeds through the participation of both adsorbed oxygen species and lattice oxygen supplied by the perovskite structure. The contribution of lattice oxygen was confirmed by methane oxidation experiments conducted in the absence of gaseous oxygen, highlighting the importance of oxygen mobility and redox properties in determining catalytic activity [77]. These results indicate that catalytic activity is governed not only by the nature of the transition-metal cation but also by the synergistic effects of cation substitution, oxygen vacancy formation, and lattice oxygen mobility. The superior performance of partially substituted perovskites demonstrates that controlled defect engineering can be more effective than simply increasing the concentration of catalytically active elements. Consequently, perovskite catalysts may outperform conventional noble-metal systems under specific reaction conditions despite their lower intrinsic metal content.

Based on numerous studies exploring the relationship between structure and catalytic performance, three general principles can be identified:

1. A wide range of A-site and B-site cation combinations can form stable perovskite structures (ABO_3);
2. Partial cation substitution promotes the formation of mixed-valence states and oxygen vacancies;
3. These structural defects strongly influence oxygen mobility, redox behavior, and catalytic activity.

Despite extensive research, no single physicochemical descriptor has been identified that universally predicts the catalytic performance of perovskite oxides. While oxygen vacancy concentration, cation valence state, and lattice oxygen mobility are frequently recognized as key parameters, their relative importance strongly depends on the reaction mechanism and operating conditions. Therefore, the rational design of advanced perovskite catalysts requires simultaneous optimization of structural stability, defect chemistry, and redox functionality rather than maximization of any individual property. These principles form the foundation for the rational design of perovskite catalysts for methane reforming, oxidation of volatile organic compounds, and CO_2 utilization. This also explains why perovskite compositions exhibiting similar crystal structures may display markedly different catalytic performances depending on synthesis conditions, defect concentrations, and microstructural characteristics. Nevertheless, direct comparison of catalytic performance reported in the literature remains challenging because activity is strongly influenced by synthesis conditions, catalyst morphology, reactor configuration, and testing protocols.

6. Application in SOFC and Oxygen Separation Membranes

A detailed analysis of the performance of perovskite-containing nanocomposite materials in oxygen separation membranes and as cathodes/anodes in solid oxide fuel cells with thin layers of electrolytes on supporting anodes is given in [55]. The main point for oxygen separa-

tion membranes is that spatially variable thin layers of perovskite+ fluorite nanocomposites supported on a NiAl foam substrate provide stable performance and high oxygen fluxes under air/methane gradients: 10 mlO_2/cm^2 min for feed 100%CH_4 at 950 °C, which is more than sufficient for practical application.

For button-size fuel cells with thin GDC/ScYSZ layers on a Ni-YSZ anode on a Ni-Al foam substrate and nanocomposite cathodes such as $LaCo_{0.4}Ni_{0.6}O_3$/GDC at 750 °C, the power density of 1200 mW/cm^2 was demonstrated for pure H_2/O_2 feeds, which is among the best values for SOFC. For these cells, the addition of a nanocomposite catalyst layer 50%LaMnCrPrO + 30% NiO + 20% YSZ on the anode from the fuel side allowed to provide stable performance and the same power density using pure H_2 or a $CH_4/2H_2O$ mixture at 700 °C. Better results were usually obtained when sintering of supported layers of electrolytes and nanocomposite cathodes and anodes was carried out using microwave sintering or sintering by electron beams.

So, these results really demonstrate highly efficient and stable performance of perovskite-fluorite nanocomposites in these devises in realistic conditions of performance.

To systematically evaluate the practical applicability of various perovskite-based materials, a comparative analysis of their performance parameters is essential. Table 2 presents representative compositions, highlighting their synthesis approaches, surface area characteristics, target reactions, catalytic activity, and long-term stability. These parameters reflect the interplay between physicochemical structure, reaction conditions, and functional performance across different applications such as oxidation reactions, fuel cells, and reforming processes. This comparison enables the identification of performance trends and structure–activity relationships, thereby offering valuable guidance for further optimization and material selection.

Table 2. Comparison of performance parameters of selected perovskite-based materials.

Material Composition	Synthesis Method	BET Surface Area (m^2/g)	Target Reaction (Temp)	Key Performance Parameter	Stability/Cycling Data	Reference
$LaCoO_3$	Sol–gel	12	CO oxidation (200 °C)	95% conv. at 220 °C	Stable for 20 h	[78]
$La_{0.6}Sr_{0.4}Co_{0.2}Fe_{0.8}O_{3-\delta}$	Molten salt	15	OER (pH 13, 1.6 V vs. RHE)	10 mA/cm^2 @ 1.58 V	Stable for 100 h	[79]
$Ba_{0.5}Sr_{0.5}Co_{0.8}Fe_{0.2}O_{3-\delta}$	Microwave-assisted	20	ORR (SOFC, 700 °C)	0.14 S/cm ionic conductivity	Retains >90% after 100 cycles	[80]
$LaFeO_{3-\delta}$	Hydrothermal	18	Methane reforming (750 °C)	CH_4 conversion: 83%	Moderate coking over 48 h	[81]
$PrBaMn_2O_{5+\delta}$	Sol–gel + calcining	8	CO oxidation (250 °C)	85% conv. at 270 °C	Minor deactivation after 24 h	[82]
$La_{0.6}Sr_{0.4}MnO_3$	Sol–gel	Not reported	CH_4 oxidation	Superior CH_4 oxidation activity compared with Pt/Al_2O_3 at low temperatures	Stable oxidation performance	[77]
$LaNiO_3$	Sol–gel	not reported	Dry reforming/reforming reactions	High reforming activity and syngas productivity	Improved coke resistance	[17–20]
$Pr_2NiO_{4+\delta}$	Pechini/combustion	Not reported	SOFC cathode/oxygen transport	High oxygen mobility and mixed ionic-electronic conductivity	Stable under long-term operation	[3,37,39,40]

The data summarized in Table 2 demonstrate that the functional performance of perovskite-based materials depends on the combined effects of composition, synthesis

route, defect chemistry, and operating conditions. Mn−, Co−, and Ni-containing compositions generally exhibit favorable redox properties for oxidation and reforming reactions, whereas Ruddlesden–Popper phases and mixed ionic–electronic conductors are particularly attractive for SOFC and membrane applications. Importantly, direct comparison between individual materials should be made cautiously because the reported performance values were obtained under different experimental conditions.

Following the comparative performance analysis presented in Table 2, a schematic illustration (Figure 6) is provided to visually summarize the interdependence between structural parameters, physicochemical properties, and catalytic/electrochemical activity in perovskite-based materials. This conceptual framework highlights how compositional tuning and defect engineering influence functional properties, which in turn dictate material performance in practical applications.

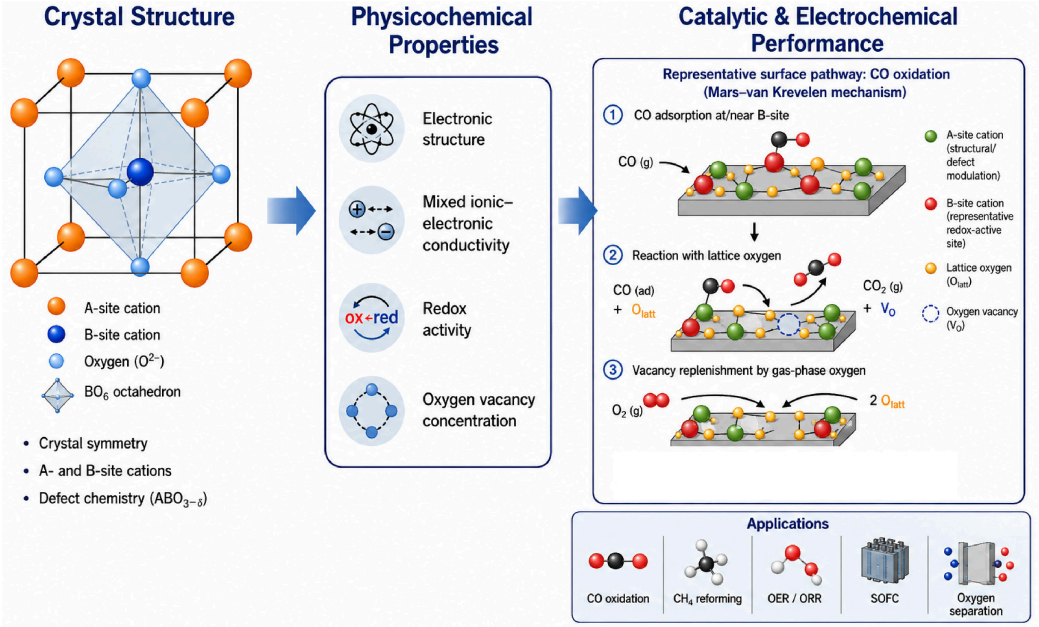

Figure 6. Relationship between crystal structure, physicochemical properties, and catalytic/electrochemical performance of perovskite oxides.

This schematic clearly illustrates how structural parameters—such as A- and B-site doping, octahedral tilting, and oxygen vacancy engineering—affect the key physicochemical properties of perovskite-based materials. These properties, in turn, determine the materials' catalytic activity, selectivity, and long-term stability in various energy-related reactions. The figure highlights the central idea of this review: optimizing structure through rational design directly enhances functional performance. This holistic understanding of structure–property–activity relationships not only explains current performance trends but also provides a conceptual foundation for the development of next-generation perovskite catalysts.

Collectively, these studies demonstrate that oxygen transport properties alone do not determine electrode performance. Instead, electrochemical activity depends on the synergistic combination of oxygen mobility, electronic conductivity, thermal compatibility, and long-term structural stability under operating conditions.

7. High-Entropy Perovskites: A New Frontier in Functional Materials

While conventional perovskite systems have demonstrated remarkable catalytic performance, their compositional limitations and structural constraints motivate the exploration

of innovative material design strategies. Among the most promising developments in this direction is the emergence of high-entropy perovskites (HEPs), which leverage configurational entropy to enable unprecedented compositional flexibility, enhanced stability, and multifunctionality. The following section discusses the structural characteristics and diverse applications of high-entropy perovskites as a new frontier in functional materials science.

High-entropy perovskites (HEPs) represent a new class of perovskite oxides in which five or more cations occupy the A- and/or B-site, generating high configurational entropy that stabilizes the crystal structure [83]. Despite retaining the conventional ABO_3 framework, HEPs exhibit enhanced lattice distortion, defect formation, and oxygen vacancy concentrations, resulting in tunable electronic, catalytic, and electrochemical properties [84,85]. These features have stimulated growing interest in their application in catalysis and energy conversion technologies.

From a thermodynamic perspective, the stabilization of high-entropy perovskites is commonly described by the configurational entropy of mixing. For a perovskite containing compositional disorder on the A- and/or B-sublattices, the ideal configurational entropy can be expressed as

$$\Delta S_{config} = -R\left[\sum_i x_i^A \ln x_i^A + \sum_j x_j^B \ln x_j^B\right] \quad (3)$$

where R is the gas constant and x_i^A and x_j^B are the mole fractions of the respective cations occupying the A- and B-sites. For an equimolar sublattice containing N cation species, the expression reduces to $\Delta S_{config} = R\,lnN$. The thermodynamic contribution of this configurational disorder to phase stability can be described through the Gibbs free energy of mixing:

$$\Delta G_{mix} = \Delta H_{mix} - T\Delta S_{config} \quad (4)$$

Thus, increasing configurational entropy can favor stabilization of a disordered single-phase perovskite at elevated temperatures; however, high ΔS_{config} alone does not guarantee phase stability. Recent thermodynamic descriptions therefore extend beyond the ideal entropy model by considering non-ideal mixing enthalpy, local lattice distortion, short-range cation ordering, oxygen defects, and non-configurational entropy contributions. Computational approaches based on density functional theory (DFT) and special quasirandom structures (SQS) are increasingly used to evaluate these contributions and predict the stability of multicomponent perovskite compositions [86,87].

HEPs have demonstrated exceptional catalytic performance, particularly in oxidation and reforming reactions. For example, Erdil and Toparli demonstrated that tuning the B-site composition in HEPOs significantly affects their bifunctional electrocatalytic performance in rechargeable zinc–air batteries [84]. Their study revealed that strategic selection of transition metal cations at the B-site enhances both oxygen reduction reaction (ORR) and oxygen evolution reaction (OER) activities, leading to improved energy efficiency and cycling stability. This work highlights the potential of compositional engineering in HEPOs to optimize catalytic behavior across different electrochemical and heterogeneous catalytic processes.

Similarly, Wang et al. reviewed the catalytic versatility of HEPs in oxygen evolution reactions (OER), where equimolar high-entropy perovskites such as $La(Cr_{0.2}Mn_{0.2}Fe_{0.2}Co_{0.2}Ni_{0.2})O_3$ outperformed traditional perovskite electrocatalysts, offering lower overpotentials and superior long-term stability. The configurational entropy inherent in HEPs enhances not only structural stability but also oxygen vacancy formation and mobility, crucial for oxidative catalysis. These findings underscore the potential of HEPs to overcome deactivation pathways, such as sintering and coking, that limit conventional perovskite catalysts [88].

In a recent study [89], catalysts based on high-entropy perovskites were developed ($La(Cr_{0.2}Mn_{0.2}Fe_{0.2}Co_{0.2}Ni_{0.2})O_3$ and $LaMnO_3$. These materials showed structural stability, moderate oxygen mobility (coefficient of oxygen diffusion D ~ 10^{-12} cm^2/s at 700 °C) and excellent coke resistance in steam reforming of ethanol. Catalysts showed an almost complete transformation of ethanol at temperatures above 700 °C and high stability under the reaction, which is associated with high dispersion of Ni particles and optimal oxygen-transport properties. The catalyst based on $La(Cr_{0.2}Mn_{0.2}Fe_{0.2}Co_{0.2}Ni_{0.2})O_3$, which ensures high activity and minimal formation of coke, even with prolonged tests, turned out to be especially promising.

The remarkable flexibility and stability of high-entropy perovskite oxides (HEPOs) have also been harnessed in electrochemical energy conversion systems, notably solid oxide fuel cells (SOFCs). Li et al. reported the development of a high-entropy perovskite cathode material designed to tolerate chromium poisoning, a major degradation mechanism in SOFCs [90]. The cathode, formulated with a complex multicomponent B-site composition, demonstrated excellent electrochemical performance and long-term stability under high-temperature operating conditions. Its high configurational entropy effectively stabilized the crystal structure and suppressed chromium deposition, maintaining catalytic activity and ionic conductivity even after extended testing. This study underscores the potential of high-entropy perovskites to overcome critical challenges in SOFC technology and paves the way for the design of durable electrodes for high-temperature electrochemical devices.

Liu et al. synthesized a high-entropy perovskite, $Pr_{1/6}La_{1/6}Nd_{1/6}Ba_{1/6}Sr_{1/6}Ca_{1/6}CoO_{3-\delta}$ (PLNBSCC), which served as an air electrode in reversible proton ceramic electrochemical cells (R-PCECs) [91]. This material exhibited outstanding bifunctional catalytic activity, achieving a peak power density of 1.21 $W{\cdot}cm^{-2}$ and an electrolysis current density of -1.95 $A{\cdot}cm^{-2}$ at 600 °C. The PLNBSCC electrode demonstrated remarkable stability and electrochemical performance, outperforming conventional perovskite-based electrodes. These results underscore the potential of configurational entropy to enhance the functionality and durability of electrochemical materials.

In photocatalysis, Wang et al. fabricated high-entropy perovskite oxides that exhibited enhanced CO_2 photoreduction activity due to the creation of abundant oxygen vacancies and improved charge carrier separation [92]. The combination of multiple cations facilitated tailored band gap engineering and light absorption across a broad spectrum. Collectively, these studies demonstrate that the primary advantage of HEPs lies not in maximizing a single performance parameter but in simultaneously optimizing structural stability, defect chemistry, oxygen mobility, and catalytic functionality [93]. The synergistic interactions among multiple cation species create opportunities for tailoring redox behavior and electronic structure beyond what is achievable in conventional perovskite systems.

Despite their considerable promise, high-entropy perovskites remain at an early stage of development. The vast compositional space complicates the establishment of clear structure–property relationships, while reproducible large-scale synthesis remains challenging. Consequently, reliable descriptors capable of predicting catalytic and electrochemical performance are still lacking [94].

Overall, high-entropy perovskites offer a transformative platform for designing advanced functional materials with exceptional stability, tunable properties, and multifunctional capabilities. Their successful implementation in catalysis, energy conversion, and electronic applications underscores the vast potential of configurational entropy as a design principle.

8. Modeling and AI-Assisted Design of Perovskite Materials

Computational modeling is playing an increasingly important role in establishing the relationships between the composition, structure, defect state, and functional properties

of perovskite oxides. At the atomistic level, density functional theory (DFT) calculations are used to estimate the electronic structure, oxygen vacancy formation energy, adsorption characteristics, and phase stability. Thermodynamic and defect-chemical models allow one to additionally take into account the influence of temperature, oxygen partial pressure, and oxygen nonstoichiometry on the equilibrium state of the material. For compositionally complex and high-entropy perovskites, DFT calculations in combination with special quasi-random structure (SQS) models allow one to evaluate the influence of the local cationic environment and compositional disorder on the stability of multicomponent phases [86,87]. However, the rapid increase in the number of possible A- and B-compositions significantly limits the application of direct atomistic calculations alone and creates a need for faster predictive approaches.

Machine-learning approaches are increasingly used to accelerate the screening and stability assessment of perovskite oxides. Representative algorithms include gradient-boosting decision trees (GBDT), random forests, Extra Trees, kernel ridge regression, deep neural networks, and symbolic-regression approaches. Input descriptors commonly include the Goldschmidt tolerance factor, octahedral factor, ionic radii, electronegativity, oxidation states, bond-length-related parameters, and other elemental or structural features. For example, a GBDT model trained on 397 ABO_3 compounds achieved 94.6% classification accuracy under 10-fold cross-validation and identified tolerance factor, octahedral factor, cation–oxygen bond characteristics, and electronegativity-related descriptors among the most important predictors of perovskite formability [95]. In a larger dataset containing more than 1900 DFT-calculated perovskite oxide energies, Extra Trees classification achieved an accuracy of 0.93 ± 0.02 and an F_1 score of 0.88 ± 0.03, while kernel ridge regression predicted the energy above the convex hull with an RMSE of 28.5 ± 7.5 meV atom^{-1} and an MAE of 16.7 ± 2.3 meV atom^{-1} [96]. More recent interpretable ML screening has extended the accessible chemical space to over one million virtual perovskite compositions, with classification accuracy of 0.919 and E regression performance of R^2 = 0.916 and RMSE = 24.2 meV atom^{-1} [97]. These models rely on experimentally compiled and/or DFT-derived datasets, including data available through resources such as the Materials Project, supplemented in some studies by systematically generated virtual compositions. Nevertheless, their predictive reliability remains dependent on dataset coverage, descriptor selection, and validation strategy; therefore, ML predictions should complement rather than replace experimental validation and physics-based calculations.

The use of artificial intelligence is gradually changing the very organization of computational materials search. In the traditional sequential approach, a promising composition is first selected by the researcher, then calculated, and then verified experimentally. AI-assisted approaches allow for the preliminary exploration of significantly broader compositional spaces and the selection of the most promising candidates for subsequent DFT calculations or experimental verification. Surrogate models can approximate the results of resource-intensive calculations and thereby reduce the number of required direct calculations, while active learning allows for the iterative selection of the most informative new compositions and the use of the obtained results for further model refinement [98]. Another developing area is physics-informed machine learning, in which physical constraints, thermodynamic relations, or governing equations are directly incorporated into the learning process [99]. Thus, the role of AI is primarily to accelerate screening, combine calculated and experimental data, and organize an iterative cycle of "prediction-validation-refinement" rather than to replace physically based modeling.

The next level is the transition from predicting material properties to modeling their behavior in a device, reactor, or process. For perovskite catalysts, membranes, and electrochemical systems, such modeling can integrate chemical kinetics with heat and mass

transfer, hydrodynamics, electrochemical processes, and material-energy balances. Commercial software packages and open platforms, which can be used to create specialized research models (Table 3), are used to solve these problems. However, these software products are not specialized simulators exclusively for perovskites: the parameters of a specific material, including reaction kinetics, transport properties, and thermodynamic characteristics, must be defined based on experimental measurements or lower-level calculations. Therefore, a promising direction is the multi-level integration of atomistic, kinetic, and process modeling, allowing the properties of a perovskite material to be linked to its behavior under real-world operating conditions [100].

Table 3. Software platforms applicable for process modeling of systems based on perovskite materials.

Platform	Type	Key Capabilities Relevant to Perovskite Systems
Aspen Plus	Commercial	Material and energy balances, reactor and process flow modeling, reforming processes, and hydrogen production
COMSOL Multiphysics	Commercial	Coupled modeling of chemical kinetics, heat and mass transfer, electrochemistry, and membrane processes
Ansys Fluent	Commercial	CFD modeling of reacting flows, surface reactions, porous media, heat and mass transfer
gPROMS Process	Commercial	Dynamic modeling of reactors and processes, parameter estimation, optimization, and scaling
Cantera/OpenFOAM	Open and customizable	Detailed chemical kinetics, thermodynamics, transport processes, and the construction of specialized research models of reacting systems

In addition to materials and process design, AI-based approaches are increasingly being applied to process monitoring and predictive maintenance. Machine-learning models can analyze real-time operational data to detect abnormal behavior, identify incipient faults, and predict equipment degradation, thereby supporting condition-based maintenance and reducing unplanned downtime. Such approaches are particularly relevant to complex chemical and energy-conversion systems, where the integration of data-driven monitoring with process models can improve operational reliability and facilitate early fault diagnosis [101].

9. Research Gaps and Future Directions

The major unresolved challenges identified across the catalytic, electrochemical, and materials applications discussed in this review are summarized in Table 4 together with the corresponding research gaps and future research priorities.

Table 4. Key research gaps and future directions for perovskite-based materials.

Research Area	Research Gap	Future Direction
Structural stability and deactivation	Phase transformations, surface reconstruction, cation segregation, sintering, and coking remain insufficiently controlled under realistic high-temperature and reactive environments [102].	Stabilize bulk and active surface states through composition, defect engineering, controlled exsolution, and long-term operando evaluation.

Table 4. *Cont.*

Research Area	Research Gap	Future Direction
Active sites and structure–function relationships	The relationships among bulk composition, oxygen nonstoichiometry, dynamically reconstructed surfaces, and reaction mechanisms remain incompletely understood.	Combine operando characterization with mechanistic modeling to identify active states and rate-controlling processes.
Synthesis and scale-up	High compositional and microstructural control achieved by laboratory synthesis is difficult to reproduce economically at larger scale [103,104].	Develop reproducible, lower-energy and scalable synthesis with reduced precursor consumption, processing steps, and batch variability.
Materials-to-device translation	Improvements observed for powders and individual compositions do not necessarily translate into structured catalysts, membranes, SOFC electrodes, or reactors.	Integrate composition and defect engineering with monoliths, membranes, porous coatings, and other structured architectures optimized for heat and mass transfer.
Benchmarking and sustainability	Non-standardized testing and limited consideration of durability, regeneration, cost, critical elements, and environmental impact hinder comparison and practical implementation.	Establish standardized long-term testing protocols and integrate durability, recyclability, safer compositions, environmental impact, and process feasibility into materials assessment.

10. Conclusions

Perovskite-like oxides represent a versatile platform for catalytic, electrochemical, and energy applications due to their combination of structural flexibility, oxygen nonstoichiometry, redox properties, and mixed ionic-electronic conductivity. Analysis shows that their functional characteristics are not determined by any single parameter. The most significant is the interrelated influence of crystal structure, defect chemistry, surface composition, microstructure, synthesis method, and operating conditions. It is particularly important to consider that characteristics such as the tolerance factor, oxygen vacancy concentration, particle size, and cation valence state cannot be considered universal, independent descriptors of activity. Their influence is determined by the specific reaction mechanism and the state of the working surface. Therefore, the rational development of perovskite materials must be based on the comprehensive optimization of structural stability, oxygen mobility, redox properties, and surface evolution under operating conditions. A comparison of synthesis methods also revealed the lack of a universally preferred approach. Mild-chemical methods provide greater control over composition and microstructure, while traditional solid-phase synthesis retains advantages in terms of reproducibility and scalability. Similarly, a comparison of catalytic, membrane, and SOFC systems confirms the need to select the composition and fabrication method based on specific applications and operating conditions.

High-entropy and layered perovskite systems expand the available compositional space and create additional opportunities for managing defect chemistry and functional properties. At the same time, the development of DFT calculations, machine learning, and AI-assisted modeling enables a transition from primarily empirical composition selection to more predictive materials design. Overall, the further development of perovskite systems will depend on the integration of experimental analysis, operando characterization, physically based modeling, and process evaluation, which will enable a more reliable link between material properties and their behavior in practical devices and processes.

Author Contributions: Conceptualization, N.T. and B.M.; methodology, G.A. and A.D.; software, A.D. and B.M.; validation, Z.M., D.K., L.N., V.S. and A.D.; formal analysis, A.K., D.K., L.N. and V.S.; investigation, G.A. and B.M.; resources, G.A., D.K. and A.K.; data curation, A.D., N.T. and Z.M.; writing—original draft preparation, N.T., A.D. and Z.M.; writing—review and editing, A.K., B.M. and V.S.; visualization, B.M.; supervision, A.D. and Z.M.; project administration, B.M. and A.D.; funding acquisition, A.D. All authors have read and agreed to the published version of the manuscript.

Funding: This research received no external funding.

Institutional Review Board Statement: The conducted research was not related to either human or animal use, where consent is required.

Data Availability Statement: All data generated or analysed during this study are included in this published article.

Acknowledgments: During the preparation of this manuscript, the authors used Claude (Anthropic, San Francisco, CA, USA) for English-language editing and grammar checking. An AI-assisted tool was used in the preparation of the schematic illustration in Figure 6. The authors reviewed and edited all AI-assisted output and take full responsibility for the scientific content of the manuscript.

Conflicts of Interest: The authors declare no conflicts of interest.

Abbreviations

The following abbreviations are used in this manuscript:

R–P	Ruddlesden–Popper
SOFC	Solid oxide fuel cell
OER	Oxygen evolution reaction
ORR	Oxygen reduction reaction
HEP	High-entropy perovskite
HEPO	High-entropy perovskite oxide
R-PCEC	Reversible proton ceramic electrochemical cell
XRD	X-ray diffraction
XPS	X-ray photoelectron spectroscopy
XANES	X-ray absorption near-edge structure
DRIFTS	Diffuse reflectance infrared Fourier transform spectroscopy
TEM	Transmission electron microscopy
EDX	Energy-dispersive X-ray spectroscopy
DFT	Density functional theory
BET	Brunauer–Emmett–Teller
GBDT	gradient-boosting decision trees
SQS	special quasirandom structures

References

1. International Energy Agency (IEA). *World Energy Outlook 2021*; IEA: Paris, France, 2021.
2. Li, W.; Sunarso, J.; Yang, Y.; Chen, Y.; Ge, C.; Wang, W.; Guo, Y.; Ran, R.; Zhou, W. Strategies for Improving Oxygen Ionic Conducting in Perovskite Oxides and Their Practical Applications. *Energy Rev.* **2024**, *3*, 100085. [CrossRef]
3. Lee, D.; Lee, H. Controlling Oxygen Mobility in Ruddlesden–Popper Oxides. *Materials* **2017**, *10*, 368. [CrossRef] [PubMed]
4. Morales-Zapata, M.A.; Larrea, A.; Laguna-Bercero, M.A. Lanthanide Nickelates for Their Application on Solid Oxide Cells. *Electrochim. Acta* **2023**, *444*, 141970. [CrossRef]
5. Atta, N.F.; Galal, A.; El-Ads, E.H. Perovskite Nanomaterials—Synthesis, Characterization, and Applications. In *Perovskite Materials—Synthesis, Characterisation, Properties, and Applications*; Pan, L., Zhu, G., Eds.; InTech: Melbourne, FL, USA, 2016.
6. Cheng, X.; Zhao, G.; Qiang, W.; Huang, B. Improvement of Electrochemical Performance and Structural Stability of $LiNi_{0.83}Co_{0.12}Mn_{0.05}O_2$ at High-Voltage by La and Ti Modification. *J. Alloys Compd.* **2022**, *908*, 164592. [CrossRef]
7. Peña, M.A.; Fierro, J.L.G. Chemical Structures and Performance of Perovskite Oxides. *Chem. Rev.* **2001**, *101*, 1981–2018. [CrossRef] [PubMed]

8. Lakshminarayanan, N.; Choi, H.; Kuhn, J.N.; Ozkan, U.S. Effect of Additional B-Site Transition Metal Doping on Oxygen Transport and Activation Characteristics in $La_{0.6}Sr_{0.4}(Co_{0.18}Fe_{0.72}X_{0.1})O_{3-\delta}$ (Where X = Zn, Ni or Cu) Perovskite Oxides. *Appl. Catal. B Environ.* **2011**, *103*, 318–325. [CrossRef]
9. Royer, S.; Duprez, D. Catalytic Oxidation of Carbon Monoxide over Transition Metal Oxides. *ChemCatChem* **2011**, *3*, 24–65. [CrossRef]
10. Zhang, J.; Li, H. (Eds.) *Perovskite: Crystallography, Chemistry and Catalytic Performance*; Geology and Mineralogy Research Developments; Nova Publishers: New York, NY, USA, 2013.
11. Yang, L.; Li, Y.; Sun, Y.; Wang, W.; Shao, Z. Perovskite Oxides in Catalytic Combustion of Volatile Organic Compounds: Recent Advances and Future Prospects. *Energy Environ. Mater.* **2022**, *5*, 751–776. [CrossRef]
12. Cimino, S.; Colonna, S.; De Rossi, S.; Faticanti, M.; Lisi, L.; Pettiti, I.; Porta, P. Methane Combustion and CO Oxidation on Zirconia-Supported La, Mn Oxides and $LaMnO_3$ Perovskite. *J. Catal.* **2002**, *205*, 309–317. [CrossRef]
13. Wang, G.; Zhang, S.; Huang, Z.; Cui, X.; Song, Z. Study of the Structure and Catalytic Activity of B-Site Doping Perovskite for an Inferior Anthracite Coal Combustion. *Energies* **2023**, *16*, 5432. [CrossRef]
14. Wu, T.; Zhang, L.; Zhan, Y.; Dong, Y.; Tan, Z.; Zhou, B.; Wei, F.; Zhang, D.; Long, X. Recent Progress on Perovskite-Based Electrocatalysts for Efficient CO_2 Reduction. *Molecules* **2023**, *28*, 8154. [CrossRef] [PubMed]
15. Gai, D.; Shi, J.; Cui, X.; Zhao, P.; Zuo, W.; Zhang, J.; Jia, G.; Huang, Z. Catalytic Performance and Mechanism of A-Site Vacancy Deficient Perovskite Catalyst over Tar Cracking during Biomass Pyrolysis. *J. Clean. Prod.* **2023**, *405*, 136876. [CrossRef]
16. Liu, C.; Zhao, Z.; Luo, J.; Xu, C.; Abuelgasim, S.; Li, T.; Xiao, Y.; Kawi, S. Hydrogen-Rich Syngas Production by the Three-Dimensional Structure of $LaNiO_3$ Catalyst from a Blend of Acetic Acid and Acetone as a Bio-Oil Model Compound. *Int. J. Hydrogen Energy* **2022**, *47*, 15160–15174. [CrossRef]
17. Wu, G.; Li, S.; Zhang, C.; Wang, T.; Gong, J. Glycerol Steam Reforming over Perovskite-Derived Nickel-Based Catalysts. *Appl. Catal. B Environ.* **2014**, *144*, 277–285. [CrossRef]
18. Marinho, A.L.A.; Rabelo-Neto, R.C.; Noronha, F.B.; Mattos, L.V. Steam Reforming of Ethanol over Ni-Based Catalysts Obtained from $LaNiO_3$ and $LaNiO_3/CeSiO_2$ Perovskite-Type Oxides for the Production of Hydrogen. *Appl. Catal. A Gen.* **2016**, *520*, 53–64. [CrossRef]
19. De Lima, S.M.; Da Silva, A.M.; Da Costa, L.O.O.; Assaf, J.M.; Mattos, L.V.; Sarkari, R.; Venugopal, A.; Noronha, F.B. Hydrogen Production through Oxidative Steam Reforming of Ethanol over Ni-Based Catalysts Derived from $La_{1-x}Ce_xNiO_3$ Perovskite-Type Oxides. *Appl. Catal. B Environ.* **2012**, *121–122*, 1–9. [CrossRef]
20. Bengaard, H.S.; Nørskov, J.K.; Sehested, J.; Clausen, B.S.; Nielsen, L.P.; Molenbroek, A.M.; Rostrup-Nielsen, J.R. Steam Reforming and Graphite Formation on Ni Catalysts. *J. Catal.* **2002**, *209*, 365–384. [CrossRef]
21. Swierczek, K.; Marzec, J.; Palubiak, D.; Zajac, W.; Molenda, J. LFN and LSCFN Perovskites—Structure and Transport Properties. *Solid State Ion.* **2006**, *177*, 1811–1817. [CrossRef]
22. Bischak, C.G.; Hetherington, C.L.; Wu, H.; Aloni, S.; Ogletree, D.F.; Limmer, D.T.; Ginsberg, N.S. Origin of Reversible Photoinduced Phase Separation in Hybrid Perovskites. *Nano Lett.* **2017**, *17*, 1028–1033. [CrossRef] [PubMed]
23. Istomin, S.Y.; Antipov, E.V. Cathode Materials Based on Perovskite-like Transition Metal Oxides for Intermediate Temperature Solid Oxide Fuel Cells. *Russ. Chem. Rev.* **2013**, *82*, 686–700. [CrossRef]
24. Ishihara, T. (Ed.) *Perovskite Oxide for Solid Oxide Fuel Cells*; Fuel Cells and Hydrogen Energy; Springer: Boston, MA, USA, 2009.
25. Aliofkhazraei, M. (Ed.) *Advances in Nanostructured Composites*; Applications of Nanocomposites; CRC Press/Taylor & Francis Group: Boca Raton, FL, USA, 2019.
26. Samreen, A.; Ali, M.S.; Huzaifa, M.; Ali, N.; Hassan, B.; Ullah, F.; Ali, S.; Arifin, N.A. Advancements in Perovskite-Based Cathode Materials for Solid Oxide Fuel Cells: A Comprehensive Review. *Chem. Rec.* **2024**, *24*, e202300247. [CrossRef] [PubMed]
27. Opitz, A.K.; Rameshan, C.; Kubicek, M.; Rupp, G.M.; Nenning, A.; Götsch, T.; Blume, R.; Hävecker, M.; Knop-Gericke, A.; Rupprechter, G.; et al. The Chemical Evolution of the $La_{0.6}Sr_{0.4}CoO_{3-\delta}$ Surface Under SOFC Operating Conditions and Its Implications for Electrochemical Oxygen Exchange Activity. *Top. Catal.* **2018**, *61*, 2129–2141. [CrossRef] [PubMed]
28. Lyu, F.; Chen, Z.; Shi, R.; Yu, J.; Lin, B.-L. Solid Phase Synthesis of Metal-Free Perovskite Crystalline Materials. *J. Solid State Chem.* **2021**, *304*, 122548. [CrossRef]
29. Nambiraj, B.; Kunka Ravindran, A.; Muthu, S.P.; Perumalsamy, R. Cost-Effective Synthesis Method: Toxic Solvent-Free Approach for Stable Mixed Cation Perovskite Powders in Photovoltaic Applications. *Small Methods* **2025**, *9*, 2400768. [CrossRef] [PubMed]
30. Molchanov, V.V.; Buyanov, R.A. Scientific Grounds for the Application of Mechanochemistry to Catalyst Preparation. *Kinet. Catal.* **2001**, *42*, 366–374. [CrossRef]
31. Sfirloaga, P.; Poienar, M.; Vlazan, P. A Review of Perovskite-Type Materials: From Synthesis to Applications. In *Environmental Remediation in Agri-Food Industry Using Nanotechnology and Sustainable Strategies*; Elsevier: Amsterdam, The Netherlands, 2025; pp. 121–139.
32. Navas, D.; Fuentes, S.; Castro-Alvarez, A.; Chavez-Angel, E. Review on Sol-Gel Synthesis of Perovskite and Oxide Nanomaterials. *Gels* **2021**, *7*, 275. [CrossRef] [PubMed]

33. Borowski, M. (Ed.) *Perovskites: Structure, Properties, and Uses*; Nova Science Publishers, Inc.: New York, NY, USA, 2010.
34. Massalimova, B.; Sadykov, V.; Totenova, N.; Fedorova, J.; Glazneva, T.; Krieger, T.; Rogov, V.; Ishchenko, A. Efficient and Stable to Coking Catalysts of Ethanol Steam Reforming Comprised of Ni + Ru Loaded on $MgAl_2O_4$ + $LnFe_{0.7}Ni_{0.3}O_3$ (Ln = La, Pr) Nanocomposites Prepared via Cost-Effective Procedure with Pluronic P123 Copolymer. *Open Chem.* **2024**, *22*, 20240118. [CrossRef]
35. Porotnikova, N.; Osinkin, D. Segregation and Interdiffusion Processes in Perovskites: A Review of Recent Advances. *J. Mater. Chem. A* **2024**, *12*, 2620–2646. [CrossRef]
36. Sadykov, V.A.; Sadovskaya, E.M.; Pikalova, E.Y.; Kolchugin, A.A.; Filonova, E.A.; Pikalov, S.M.; Eremeev, N.F.; Ishchenko, A.V.; Lukashevich, A.I.; Bassat, J.M. Transport Features in Layered Nickelates: Correlation between Structure, Oxygen Diffusion, Electrical and Electrochemical Properties. *Ionics* **2018**, *24*, 1181–1193. [CrossRef]
37. Xu, S.; Jacobs, R.; Morgan, D. Factors Controlling Oxygen Interstitial Diffusion in the Ruddlesden–Popper Oxide $La_{2-x}Sr_xNiO_{4+\delta}$. *Chem. Mater.* **2018**, *30*, 7166–7177. [CrossRef]
38. Pikalova, E.; Sadykov, V.; Tsvinkinberg, V.; Kolchugin, A.; Zhulanova, T.; Guseva, E.; Eremeev, N.; Sadovskaya, E.; Belyaev, V.; Filonova, E. Boosting the Oxygen Transport Kinetics and Functional Properties of $La_2NiO_{4+\delta}$ via Partial La-to-Sm Substitution. *J. Alloys Compd.* **2024**, *980*, 173648. [CrossRef]
39. Maksimchuk, T.; Filonova, E.; Mishchenko, D.; Eremeev, N.; Sadovskaya, E.; Bobrikov, I.; Fetisov, A.; Pikalova, N.; Kolchugin, A.; Shmakov, A.; et al. High-Temperature Behavior, Oxygen Transport Properties, and Electrochemical Performance of Cu-Substituted $Nd_{1.6}Ca_{0.4}NiO_{4+\delta}$ Electrode Materials. *Appl. Sci.* **2022**, *12*, 3747. [CrossRef]
40. Pikalova, E.; Eremeev, N.; Sadovskaya, E.; Sadykov, V.; Tsvinkinberg, V.; Pikalova, N.; Kolchugin, A.; Vylkov, A.; Baynov, I.; Filonova, E. Influence of the Substitution with Rare Earth Elements on the Properties of Layered Lanthanum Nickelate—Part 1: Structure, Oxygen Transport and Electrochemistry Evaluation. *Solid State Ion.* **2022**, *379*, 115903. [CrossRef]
41. Sadykov, V.A.; Sadovskaya, E.M.; Bespalko, Y.N.; Smal', E.A.; Eremeev, N.F.; Prosvirin, I.P.; Bulavchenko, O.A.; Mikhailenko, M.A.; Korobeynikov, M.V. Structural, Surface and Oxygen Transport Properties of Sm-Doped Nd Nickelates. *Solid State Ion.* **2024**, *412*, 116596. [CrossRef]
42. Liu, L.-B.; Yi, C.; Mi, H.-C.; Zhang, S.L.; Fu, X.-Z.; Luo, J.-L.; Liu, S. Perovskite Oxides Toward Oxygen Evolution Reaction: Intellectual Design Strategies, Properties and Perspectives. *Electrochem. Energy Rev.* **2024**, *7*, 14. [CrossRef] [PubMed]
43. Zheng, H.; Jiang, X.; Gao, Y.; Tong, A.; Zeng, L. Chemical Looping Reforming: Process Fundamentals and Oxygen Carriers. *Discov. Chem. Eng.* **2022**, *2*, 5. [CrossRef]
44. Ruh, T.; Berkovec, D.; Schrenk, F.; Rameshan, C. Exsolution on Perovskite Oxides: Morphology and Anchorage of Nanoparticles. *Chem. Commun.* **2023**, *59*, 3948–3956. [CrossRef] [PubMed]
45. Kim, Y.H.; Jeong, H.; Won, B.-R.; Jeon, H.; Park, C.; Park, D.; Kim, Y.; Lee, S.; Myung, J. Nanoparticle Exsolution on Perovskite Oxides: Insights into Mechanism, Characteristics and Novel Strategies. *Nano-Micro Lett.* **2024**, *16*, 33. [CrossRef] [PubMed]
46. Hu, Z.; Yan, Q.; Wang, Y. Dynamic Surface Reconstruction of Perovskite Oxides in Oxygen Evolution Reaction and Its Impacts on Catalysis: A Critical Review. *Mater. Today Chem.* **2023**, *34*, 101800. [CrossRef]
47. Hjiri, M.; Mustapha, N. Perovskite Oxide Catalysts: Molecular-Level Design, Structure–Activity Relationships, and Reaction Mechanisms. *Mol. Catal.* **2026**, *595*, 115844. [CrossRef]
48. Isupova, L.; Rogov, V.; Gerasimov, E.; Prosvirin, I. Influence of the $LaMn_{1-x}Fe_xO_3$ (x = 0–1) Composition on Catalytic Activities in the Reactions Involving Oxygen. *Catalysts* **2022**, *12*, 1563. [CrossRef]
49. Bartel, C.J.; Sutton, C.; Goldsmith, B.R.; Ouyang, R.; Musgrave, C.B.; Ghiringhelli, L.M.; Scheffler, M. New Tolerance Factor to Predict the Stability of Perovskite Oxides and Halides. *Sci. Adv.* **2019**, *5*, eaav0693. [CrossRef]
50. Yamada, I.; Takamatsu, A.; Ikeno, H. Complementary Evaluation of Structure Stability of Perovskite Oxides Using Bond-Valence and Density-Functional-Theory Calculations. *Sci. Technol. Adv. Mater.* **2018**, *19*, 101–107. [CrossRef] [PubMed]
51. Cho, J.; Kim, M.; Yang, I.; Park, K.T.; Rhee, C.H.; Park, H.W.; Jung, J.C. Oxygen Vacancy Engineering for Tuning the Catalytic Activity of $LaCoO_3$ Perovskite. *J. Rare Earths* **2024**, *42*, 506–514. [CrossRef]
52. Yu, J.; Li, H.; Lin, N.; Gong, Y.; Jiang, H.; Chen, J.; Wang, Y.; Zhang, X. Oxygen-Deficient Engineering for Perovskite Oxides in the Application of AOPs: Regulation, Detection, and Reduction Mechanism. *Catalysts* **2023**, *13*, 148. [CrossRef]
53. Georgiadis, A.G.; Charisiou, N.D.; Goula, M.A. A Mini-Review on Lanthanum–Nickel-Based Perovskite-Derived Catalysts for Hydrogen Production via the Dry Reforming of Methane (DRM). *Catalysts* **2023**, *13*, 1357. [CrossRef]
54. Zheng, Y.; Li, K.; Wang, H.; Tian, D.; Wang, Y.; Zhu, X.; Wei, Y.; Zheng, M.; Luo, Y. Designed Oxygen Carriers from Macroporous $LaFeO_3$ Supported CeO_2 for Chemical-Looping Reforming of Methane. *Appl. Catal. B Environ.* **2017**, *202*, 51–63. [CrossRef]
55. Sikstrom, D.; Thangadurai, V. A Tutorial Review on Solid Oxide Fuel Cells: Fundamentals, Materials, and Applications. *Ionics* **2026**, *32*, 5–30. [CrossRef] [PubMed]
56. Arapova, M.; Naurzkulova, S.; Krieger, T.; Rogov, V.; Sadykov, V. Efficient Catalysts of Ethanol Steam Reforming Based on Perovskite-Fluorite Nanocomposites with Supported Ni: Effect of the Synthesis Methods on the Activity and Stability. *Catalysts* **2022**, *12*, 1151. [CrossRef]

57. Pham, T.N.; Andrea Choi Tan, B.; Hamamoto, Y.; Inagaki, K.; Hamada, I.; Morikawa, Y. Stability of Pd_xO_y Particles Supported on Strontium Titanate Perovskite under Three-Way Catalyst Operating Conditions: Implications for Sintering Resistance. *ACS Catal.* **2024**, *14*, 1443–1458. [CrossRef]
58. Benedek, N.A.; Fennie, C.J. Hybrid Improper Ferroelectricity: A Mechanism for Controllable Polarization-Magnetization Coupling. *Phys. Rev. Lett.* **2011**, *106*, 107204. [CrossRef] [PubMed]
59. Suntivich, J.; May, K.J.; Gasteiger, H.A.; Goodenough, J.B.; Shao-Horn, Y. A Perovskite Oxide Optimized for Oxygen Evolution Catalysis from Molecular Orbital Principles. *Science* **2011**, *334*, 1383–1385. [CrossRef] [PubMed]
60. Lee, Y.-L.; Kleis, J.; Rossmeisl, J.; Shao-Horn, Y.; Morgan, D. Prediction of Solid Oxide Fuel Cell Cathode Activity with First-Principles Descriptors. *Energy Environ. Sci.* **2011**, *4*, 3966–3970. [CrossRef]
61. Hong, W.T.; Stoerzinger, K.A.; Lee, Y.-L.; Giordano, L.; Grimaud, A.; Johnson, A.M.; Hwang, J.; Crumlin, E.J.; Yang, W.; Shao-Horn, Y. Charge-Transfer-Energy-Dependent Oxygen Evolution Reaction Mechanisms for Perovskite Oxides. *Energy Environ. Sci.* **2017**, *10*, 2190–2200. [CrossRef]
62. Tsuji, M.; Hashimoto, M.; Nishizawa, Y.; Kubokawa, M.; Tsuji, T. Microwave-Assisted Synthesis of Metallic Nanostructures in Solution. *Chem. A Eur. J.* **2005**, *11*, 440–452. [CrossRef] [PubMed]
63. Gaikwad, V.M.; Sheikh, J.R.; Acharya, S.A. Investigation of Photocatalytic and Dielectric Behavior of $LaFeO_3$ Nanoparticles Prepared by Microwave-Assisted Sol–Gel Combustion Route. *J. Sol-Gel Sci. Technol.* **2015**, *76*, 27–35. [CrossRef]
64. Zhang, Y.; Luo, D.; Zhang, Y.; Lv, J. Effect of Synthesis Methods on the Electrochemical Performance of Perovskite-type $La0.6Sr0.4Co0.2Fe0.8O_3$ as Supercapacitor Electrode Material. *Ionics* **2025**, *31*, 9567–9580. [CrossRef]
65. Levitas, B.; Piligian, S.; Ireland, T.; Gopalan, S. Elucidating the Influence of Molten Salt Chemistries on the Synthesis and Stability of Perovskites Oxides. *RSC Adv.* **2021**, *11*, 29156–29163. [CrossRef] [PubMed]
66. Bhavisha, M.; Anjali, K.; Aswani, S.; Sakthivel, A. Catalytic Applications of Perovskites. In *Ceramic Catalysts*; Elsevier: Amsterdam, The Netherlands, 2023; pp. 19–55.
67. Keav, S.; Matam, S.; Ferri, D.; Weidenkaff, A. Structured Perovskite-Based Catalysts and Their Application as Three-Way Catalytic Converters—A Review. *Catalysts* **2014**, *4*, 226–255. [CrossRef]
68. Lincheng, X.; Yue, W.; Yong, Y.; Zhanzhong, H.; Xin, C.; Fan, L. Optimisation of the Electronic Structure by Rare Earth Doping to Enhance the Bifunctional Catalytic Activity of Perovskites. *Appl. Energy* **2023**, *339*, 120931. [CrossRef]
69. Zhang, W.W.; Wang, Y.; Li, Y.C.; Zhang, X.Y. Investigation into Electrochemical Catalytic Properties and Electronic Structure of Mn Doped $SrCoO_3$ Perovskite Catalysts. *J. Ind. Eng. Chem.* **2024**, *139*, 199–212. [CrossRef]
70. López, E.; Divins, N.J.; Anzola, A.; Schbib, S.; Borio, D.; Llorca, J. Ethanol Steam Reforming for Hydrogen Generation over Structured Catalysts. *Int. J. Hydrogen Energy* **2013**, *38*, 4418–4428. [CrossRef]
71. González-Gil, R.; Herrera, C.; Larrubia, M.A.; Mariño, F.; Laborde, M.; Alemany, L.J. Hydrogen Production by Ethanol Steam Reforming over Multimetallic $RhCeNi/Al_2O_3$ Structured Catalyst. Pilot-Scale Study. *Int. J. Hydrogen Energy* **2016**, *41*, 16786–16796. [CrossRef]
72. Casanovas, A.; De Leitenburg, C.; Trovarelli, A.; Llorca, J. Catalytic Monoliths for Ethanol Steam Reforming. *Catal. Today* **2008**, *138*, 187–192. [CrossRef]
73. Goyal, N.; Pant, K.K.; Gupta, R. Hydrogen Production by Steam Reforming of Model Bio-Oil Using Structured Ni/Al_2O_3 Catalysts. *Int. J. Hydrogen Energy* **2013**, *38*, 921–933. [CrossRef]
74. Salge, J.; Deluga, G.; Schmidt, L. Catalytic Partial Oxidation of Ethanol over Noble Metal Catalysts. *J. Catal.* **2005**, *235*, 69–78. [CrossRef]
75. Lónyi, F.; Valyon, J.; Someus, E.; Hancsók, J. Steam Reforming of Bio-Oil from Pyrolysis of MBM over Particulate and Monolith Supported $Ni/\gamma\text{-}Al_2O_3$ Catalysts. *Fuel* **2013**, *112*, 23–30. [CrossRef]
76. Williams, J.L. Monolith Structures, Materials, Properties and Uses. *Catal. Today* **2001**, *69*, 3–9. [CrossRef]
77. Isupova, L.A.; Tsybulya, S.V.; Kryukova, G.N.; Alikina, G.M.; Boldyreva, N.N.; Yakovleva, I.S.; Ivanov, V.P.; Sadykov, V.A. Real Structure and Catalytic Activity of La1−Ca MnO_3+ Perovskites. *Solid State Ion.* **2001**, *141–142*, 417–425. [CrossRef]
78. Sanz, O.; Banús, E.D.; Goya, A.; Larumbe, H.; Delgado, J.J.; Monzón, A.; Montes, M. Stacked Wire-Mesh Monoliths for VOCs Combustion: Effect of the Mesh-Opening in the Catalytic Performance. *Catal. Today* **2017**, *296*, 76–83. [CrossRef]
79. Sunarso, J.; Hashim, S.S.; Zhu, N.; Zhou, W. Perovskite Oxides Applications in High Temperature Oxygen Separation, Solid Oxide Fuel Cell and Membrane Reactor: A Review. *Prog. Energy Combust. Sci.* **2017**, *61*, 57–77. [CrossRef]
80. Huamán, J.L.C.; Sczancoski, J.C.; Marega, E.; Pinto, A.H. Methods for the Synthesis of Ceramic Materials with Perovskite Structure. In *Perovskite Ceramics*; Elsevier: Amsterdam, The Netherlands, 2023; pp. 31–75.
81. Ahmadi-Kashani, M.; Zendehdel, M.; Schirone, L.; Abolhasani, M.M.; Yaghoobi Nia, N. Recent Progress in the Use of Perovskites for Electrochemical, Photoelectrochemical, and Photovoltaic–Electrochemical CO_2 Reduction. *Energies* **2023**, *16*, 7632. [CrossRef]
82. Torregrosa-Rivero, V.; Sánchez-Adsuar, M.-S.; Illán-Gómez, M.-J. Analyzing the Role of Copper in the Soot Oxidation Performance of $BaMnO_3$-Perovskite-Based Catalyst Obtained by Modified Sol-Gel Synthesis. *Fuel* **2022**, *328*, 125258. [CrossRef]

83. Rost, C.M.; Sachet, E.; Borman, T.; Moballegh, A.; Dickey, E.C.; Hou, D.; Jones, J.L.; Curtarolo, S.; Maria, J.-P. Entropy-Stabilized Oxides. *Nat. Commun.* **2015**, *6*, 8485. [CrossRef] [PubMed]
84. Erdil, T.; Toparli, C. B-Site Effect on High-Entropy Perovskite Oxide as a Bifunctional Electrocatalyst for Rechargeable Zinc–Air Batteries. *ACS Appl. Energy Mater.* **2023**, *6*, 11255–11267. [CrossRef]
85. Folgueras, M.C.; Jiang, Y.; Jin, J.; Yang, P. High-Entropy Halide Perovskite Single Crystals Stabilized by Mild Chemistry. *Nature* **2023**, *621*, 282–288. [CrossRef] [PubMed]
86. Ma, J.; Liu, T.; Ye, W.; He, Q.; Chen, K. High-Entropy Perovskite Oxides for Energy Materials: A Review. *J. Energy Storage* **2024**, *90*, 111890. [CrossRef]
87. Tiwtusthada, S.; Saelee, T.; Khajondetchairit, P.; Rittiruam, M.; Praserthdam, P.; Praserthdam, S. The Development of Configurational Entropy Formulation for High-Entropy Oxides: Review and Outlook. *J. Alloys Compd.* **2025**, *1037*, 182599. [CrossRef]
88. Wang, Y.; Robson, M.J.; Manzotti, A.; Ciucci, F. High-Entropy Perovskites Materials for next-Generation Energy Applications. *Joule* **2023**, *7*, 848–854. [CrossRef]
89. Eremeev, N.F.; Hanna, S.A.; Sadovskaya, E.M.; Leonova, A.A.; Bulavchenko, O.A.; Ishchenko, A.V.; Prosvirin, I.P.; Sadykov, V.A.; Bespalko, Y.N. Catalysts for Ethanol Dry Reforming Based on High-Entropy Perovskites. *J. Catal.* **2025**, *445*, 116028. [CrossRef]
90. Li, Z.; Guan, B.; Xia, F.; Nie, J.; Li, W.; Ma, L.; Li, W.; Zhou, L.; Wang, Y.; Tian, H.; et al. High-Entropy Perovskite as a High-Performing Chromium-Tolerant Cathode for Solid Oxide Fuel Cells. *ACS Appl. Mater. Interfaces* **2022**, *14*, 24363–24373. [CrossRef] [PubMed]
91. Liu, Z.; Tang, Z.; Song, Y.; Yang, G.; Qian, W.; Yang, M.; Zhu, Y.; Ran, R.; Wang, W.; Zhou, W.; et al. High-Entropy Perovskite Oxide: A New Opportunity for Developing Highly Active and Durable Air Electrode for Reversible Protonic Ceramic Electrochemical Cells. *Nano-Micro Lett.* **2022**, *14*, 217. [CrossRef] [PubMed]
92. Wang, M.; Li, L.; Li, Y.; Shi, X.; Ren, H.; Sun, Y.; Liu, K.; Song, W.; Li, H.; Wang, H.; et al. Entropy Engineering of La-Based Perovskite for Simultaneous Photocatalytic CO_2 Reduction and Biomass Oxidation. *Chem. Commun.* **2023**, *59*, 14673–14676. [CrossRef] [PubMed]
93. Sarkar, A.; Wang, Q.; Schiele, A.; Chellali, M.R.; Bhattacharya, S.S.; Wang, D.; Brezesinski, T.; Hahn, H.; Velasco, L.; Breitung, B. High-Entropy Oxides: Fundamental Aspects and Electrochemical Properties. *Adv. Mater.* **2019**, *31*, 1806236. [CrossRef] [PubMed]
94. Oses, C.; Toher, C.; Curtarolo, S. High-Entropy Ceramics. *Nat. Rev. Mater.* **2020**, *5*, 295–309. [CrossRef]
95. Li, Z.; Mao, X.; Feng, D.; Li, M.; Xu, X.; Luo, Y.; Zhuang, L.; Lin, R.; Zhu, T.; Liang, F.; et al. Prediction of Perovskite Oxygen Vacancies for Oxygen Electrocatalysis at Different Temperatures. *Nat. Commun.* **2024**, *15*, 9318. [CrossRef] [PubMed]
96. Liu, H.; Cheng, J.; Dong, H.; Feng, J.; Pang, B.; Tian, Z.; Ma, S.; Xia, F.; Zhang, C.; Dong, L. Screening Stable and Metastable ABO_3 Perovskites Using Machine Learning and the Materials Project. *Comput. Mater. Sci.* **2020**, *177*, 109614. [CrossRef]
97. Zhao, J.; Wang, X.; Li, H.; Xu, X. Interpretable Machine Learning-Assisted Screening of Perovskite Oxides. *RSC Adv.* **2024**, *14*, 3909–3922. [CrossRef] [PubMed]
98. Merchant, A.; Batzner, S.; Schoenholz, S.S.; Aykol, M.; Cheon, G.; Cubuk, E.D. Scaling Deep Learning for Materials Discovery. *Nature* **2023**, *624*, 80–85. [CrossRef] [PubMed]
99. Meng, C.; Griesemer, S.; Cao, D.; Seo, S.; Liu, Y. When Physics Meets Machine Learning: A Survey of Physics-Informed Machine Learning. *Mach. Learn. Comput. Sci. Eng.* **2025**, *1*, 20. [CrossRef]
100. Wang, R.; Li, Z.; Liu, L. Multiscale Modeling for the Reduction Kinetics of a Perovskite Oxygen Carrier Based on Quantum Chemistry and CFD–DEM. *Carbon Capture Sci. Technol.* **2025**, *14*, 100357. [CrossRef]
101. Hameed, S.; Bigdeli, A.; El Messaoudi, N.; Starčević, S.; Sharma, A.; Teoh, Y.H.; Nemţanu, M.R.; Khzouz, M. Artificial Intelligence in Chemical Engineering Process Monitoring and Predictive Maintenance. In *Artificial Intelligence in Chemical Engineering*; Elsevier: Amsterdam, The Netherlands, 2026; pp. 287–311.
102. Stojanovic, B.D. Mechanochemical Synthesis of Ceramic Powders with Perovskite Structure. *J. Mater. Process. Technol.* **2003**, *143–144*, 78–81. [CrossRef]
103. Grabowska, E. Selected Perovskite Oxides: Characterization, Preparation and Photocatalytic Properties—A Review. *Appl. Catal. B Environ.* **2016**, *186*, 97–126. [CrossRef]
104. Xia, W.; Lu, Y.; Zhu, X. Preparation Methods of Perovskite-Type Oxide Materials. In *Revolution of Perovskite*; Arul, N.S., Nithya, V.D., Eds.; Materials Horizons: From Nature to Nanomaterials; Springer: Singapore, 2020; pp. 61–93.

Disclaimer/Publisher's Note: The statements, opinions and data contained in all publications are solely those of the individual author(s) and contributor(s) and not of MDPI and/or the editor(s). MDPI and/or the editor(s) disclaim responsibility for any injury to people or property resulting from any ideas, methods, instructions or products referred to in the content.